https://doi.org/10.5194/egusphere-2024-3749
Preprint. Discussion started: 9 December 2024

New insights into the polar ozone and water vapor, radiative effects, and their connection to the tides in the mesosphere-lower thermosphere during major Sudden Stratospheric Warming events

Guochun Shi[1,2], Hanli Liu[3], Masaki Tsutsumi[4,5], Njål Gulbrandsen[6], Alexander Kozlovsky[7], Dimitry Pokhotelov[8], Mark Lester[9], Kun Wu[3,*], and Gunter Stober[1,2]

[1]Oeschger Center for Climate Change Research, University of Bern, Bern, Switzerland
[2]Institute of Applied Physics, University of Bern, Bern, Switzerland
[3]High Altitude Observatory, National Center for Atmospheric Research, Boulder, CO, USA
[4]National Institute of Polar Research, Tachikawa, Japan
[5]The Graduate University for Advanced Studies (SOKENDAI), Tokyo, Japan
[6]Tromsø Geophysical Observatory UiT - The Arctic University of Norway, Tromsø, Norway
[7]Sodankylä Geophysical Observatory, University of Oulu, Finland
[8]Potsdam Institute for Climate Impact Research, Member of the Leibniz Association, Potsdam, Germany
[9]Department of Physics and Astronomy, University of Leicester, Leicester, UK
[*]Now: School of Physics and Electronic Sciences, Changsha University of Science and Technology, Changsha, China

Correspondence: Guochun Shi (guochun.shi@unibe.ch)

Abstract. We examine the variability of diurnal (DT), semidiurnal (SDT), and terdiurnal (TDT) tide amplitudes in the Arctic mesosphere and lower thermosphere (MLT) during and after sudden stratospheric warming (SSW) events using meteor radar data at three polar-latitude stations: Sodankylä (67.37°N, 26.63°E), Tromsø (69.58°N, 19.22°E), and Svalbard (78.99°N, 15.99°E). By combining tidal amplitude anomalies with trace gas variations, induced by large-scale dynamical changes caused by the breaking of planetary waves, this study provides new observational insights into the variation of ozone and water vapor, transport, and tides at polar latitude. We use short-wave (QRS) and long-wave (QRL) radiative heating and cooling rates simulated by the WACCM-X model to investigate the roles of polar ozone and water vapor in linking mesospheric tidal variability during SSWs in the polar regions. Our analysis reveals distinct tidal responses during SSW events. At the onset of SSWs, a significant negative anomaly in TDT amplitudes is observed, with a decrease of 3-4 m/s, approximately 15–20% change compared to mean TDT tide. Meanwhile, SDT shows a positive anomaly of 10 m/s, with changes reaching up to 40%, indicating an enhancement of tidal amplitude. The DT amplitude exhibits a delayed enhancement, with a positive amplitude anomaly of up to 5 m/s in the meridional wind component, occurring approximately 20 days after the onset of SSWs. A similar, but weaker effect is observed in the zonal wind component, with changes reaching up to 30% in the zonal component and 50% in the meridional wind component. We analyzed the contributions of ozone and water vapor to the short-wave heating and long-wave cooling before, during, and after the onset of SSW events. Our findings suggest that the immediate responses of SDT are most likely driven by dynamical effects accompanied by the radiative effects from ozone. Radiative forcing change during SSW likely plays a secondary role in DT tidal changes but appears to be important 20 days after the event towards the spring transition. Water vapor acts as a dynamical tracer in the stratosphere and mesosphere but has minimal radiative

https://doi.org/10.5194/egusphere-2024-3749
Preprint. Discussion started: 9 December 2024

forcing, resulting in a negligible impact on tidal changes. The interaction between dynamic processes and the transport of radiatively active gases is important for explaining the observed tidal variability during SSW events. This study provides the first comprehensive analysis of mesospheric tidal variability in polar regions during SSWs, exploring and linking the significant role of trace gases and radiative effects in modulating tidal dynamics.

1 Introduction

Major SSW events are dramatic disruptions of the winter polar stratosphere, characterized by rapid temperature increases and the reversal of the typical westerly winds. These events occur due to the interaction between the planetary waves propagating from the troposphere into the stratosphere and the stratospheric mean circulation (Matsuno, 1971; Andrews et al., 1987). This interaction leads to the weakening or splitting of the winter stratospheric polar vortex (Haynes et al., 1991; Matthias et al., 2013), resulting in circulation reversal, increased downwelling in the polar stratosphere, and a subsequent rise in temperature due to adiabatic heating. SSWs have broad impacts, influencing surface temperature (Davis et al., 2022; Hall et al., 2021), weather patterns in the troposphere (Baldwin et al., 2021; Domeisen et al., 2020), large-scale circulation (Iida et al., 2014), stratospheric transport and composition (de la Cámara et al., 2018; Schranz et al., 2020; Shi et al., 2024), altering the behavior of atmospheric tides in the MLT regions (Becker, 2017; Zhang et al., 2021; Liu et al., 2022), and up to the ionosphere (Fang et al., 2012; Pedatella and Liu, 2013; Günzkofer et al., 2022).

Several observational and numerical studies have established that the occurrence of SSW events influences the tidal variabilities in the MLT across equatorial latitudes (Sridharan et al., 2009; Lima et al., 2012; Jin et al., 2012; Sathishkumar and Sridharan, 2013; Siddiqui et al., 2018; Liu et al., 2021), as well as middle and polar latitudes (Jacobi et al., 1999; Bhattacharya et al., 2004; Hoffmann et al., 2007; Pedatella et al., 2014; Chau et al., 2015; Stober et al., 2020; Liu et al., 2021; Eswaraiah et al., 2018; Hibbins et al., 2019; Zhang et al., 2021; Dempsey et al., 2021; Liu et al., 2022; van Caspel et al., 2023; Dutta et al., 2024). For instance, van Caspel et al. (2023) used a mechanistic tidal model to investigate the response of SDT to the 2013 SSW event and compared their findings with meteor radar wind observations at three stations: CMOR (43.3°N, 80.8°W), Collm (51.3°N, 13.0°E), and Kiruna (67.5°N, 20.1°E). Hibbins et al. (2019) observed an enhancement in the mid-latitude migrating SDT in the MLT regions around 10–17 days after the SSW onset using meteor wind data from the Super Dual Auroral Radar Network (SuperDARN) in the Northern Hemisphere. Dutta et al. (2024) reported an increase in solar SDT amplitude in the polar MLT regions during the boreal SSW event of 2013 and the austral SSW event of 2019. Additionally, Sathishkumar and Sridharan (2013) found a significant enhancement of DT amplitude in the zonal wind and the strength of the equatorial electrojet just before the onset of SSW, with the solar SDT dominating over the DT during the SSW.

Previous studies have suggested that the primary mechanisms driving SDT variability in the MLT during SSWs include modified zonal mean zonal winds in the stratosphere and mesosphere, and the nonlinear interaction between tides and planetary waves (Liu et al., 2010; Pedatella and Forbes, 2010; Lima et al., 2012; Jin et al., 2012; Eswaraiah et al., 2018; He and Chau, 2019; He et al., 2020; van Caspel et al., 2023). For instance, Lima et al. (2012) demonstrated that the intensified tides and quasi-two-day wave amplitudes observed during a major SSW event are associated with heightened planetary wave activity in the

https://doi.org/10.5194/egusphere-2024-3749
Preprint. Discussion started: 9 December 2024

stratospheric winter of the Northern Hemisphere. Given that the absorption of solar ultraviolet radiation (UV) by stratospheric ozone is the primary source of SDT (Forbes and Garrett, 1978; Lindzen and Chapman, 1969), and that SSWs affect the distribution of stratospheric ozone and its vertical structure of the volume mixing ratio (VMR), changes in ozone density could potentially influence the enhancement of SDT during SSW (Goncharenko et al., 2012; Pedatella et al., 2014; Limpasuvan et al., 2016; Eswaraiah et al., 2018; Stober et al., 2020; van Caspel et al., 2023). Goncharenko et al. (2012) reported that the prolonged increase in tropical ozone density around peak ozone heating rates generated a migrating semidiurnal tide, while circulation changes amplified longitudinal inhomogeneities in ozone distribution, potentially leading to the generation of non-migrating tides. Limpasuvan et al. (2016) suggested that the migrating SDT is globally amplified during the 20–30 days interval following SSW onset, likely due to enhanced stratospheric ozone in the tropics and associated solar heating linked to equatorial upwelling and cooling caused by the SSW. Eswaraiah et al. (2018) studied ozone dynamics over Antarctica and explored the nonlinear interaction between planetary waves and tides to understand tidal enhancement observed 3 to 4 weeks after the central day of SSWs. Moreover, Siddiqui et al. (2019) utilized WACCM simulations to investigate tidal amplitudes during the 2009 SSW event, highlighting the crucial role stratospheric ozone variability plays in modulating semidiurnal solar tidal changes.

While the nonlinear interaction between tides and planetary waves is considered a primary cause of SDT enhancement in the MLT region, the impact of stratospheric ozone and water vapor on tidal changes during SSW events has been studied more extensively in tropical regions than in polar regions (Flury et al., 2009; Schranz et al., 2020; Bahramvash Shams et al., 2022; Oehrlein et al., 2020; de la Cámara et al., 2018; Hong and Reichler, 2021). Motivated by the observed links between trace gas variations in tropical regions during SSWs and changes in wave-tidal amplitudes in the MLT, this study aims to explore how trace gases, specifically ozone and water vapor, change in polar regions and their potential influence on tidal amplitudes during SSW events.

In this study, we examine the causes of mesospheric tide variability in the polar regions during SSWs, specifically focusing on the role of radiative effects from ozone and water vapor. We use long-term MLT wind measurements from meteor radars at northern polar-latitude stations: Sodankylä (67.37°N, 26.63°E), Tromsø (69.58°N, 19.22°E), and Svalbard (78.99°N, 15.99°E) to analyze the variability of DT, SDT, and TDT in the zonal and meridional wind components compositing 9 major SSW events from 2004 to 2022. We utilize the QRS and QRL radiative heating and cooling rates simulated by the Specified Dynamics Whole Atmosphere Community Climate Model with thermosphere and ionosphere extension (SD-WACCM-X) to quantify, for the first time, the impact of ozone and water vapor responses on tidal variations in the MLT region This study presents a quantification of total radiative forcing changes during SSW events, and their close correspondence with ozone and water vapor changes observed at polar latitudes. Previous studies already compared SD-WACCM-X tides and mean meteor radar winds together with other GCMs (Stober et al., 2021b). The combined analysis of tidal amplitude anomalies and trace gas variations in the polar regions provides new insights into the factors influencing tidal dynamics during SSWs.

The manuscript is structured as follows. Section 2 describes the data and methodology used in this study. The results from observations and simulations are presented in Section 3, followed by the discussion in Section 4 and conclusions in Section 5.

https://doi.org/10.5194/egusphere-2024-3749
Preprint. Discussion started: 9 December 2024

2 Data and Methodology

2.1 Meteor radar data and analysis

Meteor radar observations collected at three different high latitudes are located at Svalbard (78.99°N, 15.99°E), Tromsø (69.58°N, 19.22°E), and Sodankylä (67.37°N, 26.63°E) in the Arctic. All systems were almost continuously in operation for measuring zonal and meridional winds in the MLT region with a temporal resolution of 1 h and vertical resolution of 2 km which use the same wind retrieval algorithm (Stober et al., 2021a, b). The wind retrieval algorithm is a further development of the wind analysis introduced by Hocking et al. (2001) and Holdsworth et al. (2004). The total tidal amplitude and phases are estimated using the adaptive spectral filter (ASF2D) (Baumgarten and Stober, 2019; Stober et al., 2020; Krochin et al., 2024). The total tides, usually dominated by migrating (DW1, SW2, TW3) tidal components, are obtained using the following function:

$$T(t), u(t), v(t) = T_0, u_0, v_0 + \sum_{n=1}^{3} \left[A_n \sin\left(\frac{2\pi}{P_n} t\right) + B_n \cos\left(\frac{2\pi}{P_n} t\right) \right] \quad (1)$$

Where T, u, and v are the temperature, zonal and meridional winds, respectively. P_n is 8, 12 and 24 h, corresponding to terdiurnal tides (TDT), semidiurnal tides (SDT) and diurnal tides (DT), respectively. A_n and B_n denote the Fourier coefficients for the tidal amplitudes. The zonal mean zonal and meridional wind and the zonal mean temperature are given by T_0, u_0, and v_0, respectively. The retrieval function also includes longer period waves such as the quasi-two-day wave (QTDW) and stationary planetary (Baumgarten and Stober, 2019; Schranz et al., 2020).

2.2 GROMOS-C

GROMOS-C (GRound-based Ozone MOnitoring System for Campaigns) is an ozone microwave radiometer that measures the ozone emission line at 110.836 GHz at Ny-Ålesund, Svalbard (78.99° N, 12° E) since September 2015. It was built by the Institute of Applied Physics at the University of Bern (Fernandez et al., 2015). Measured ozone profiles are retrieved from the ozone spectra with a temporal averaging of 2 hours leveraging the Atmospheric Radiative Transfer Simulator version-2 (ARTS2; Eriksson et al., 2011) and Qpack2 software (Eriksson et al., 2005) according to the optimal estimation algorithm (Rodgers, 2000). The retrieved ozone profile has a time resolution of 2 hours and a vertical resolution of 10-12 km in the stratosphere and up to 20 km in the mesosphere covering an altitude range from 23 to 70 km. The measured datasets were used to study the photochemically induced diurnal cycle of ozone in the stratosphere and lower mesosphere (Schranz et al., 2018). The ozone measurements of GROMOS-C have been validated to AURA-MLS and MERRA-2 (Schranz et al., 2020; Shi et al., 2023, 2024). Furthermore, GROMOS-C has proved capable of measuring the tertiary ozone layer above Ny-Ålesund, Svalbard in winter (Schranz et al., 2018).

https://doi.org/10.5194/egusphere-2024-3749
Preprint. Discussion started: 9 December 2024

2.3 MIAWARA-C

MIAWARA-C (MIddle Atmospheric WAter vapor RAdiometer for Campaigns) is a ground-based microwave radiometer measuring the pressure-broadened rotational emission line of water vapor at the frequency of 22 GHz. The University of Bern built this instrument (Straub et al., 2010) and performed a campaign at Ny-Ålesund, Svalbard (78.99° N, 12° E) since September 2015. MIAWARA-C retrieval, like GROMOS-C, is conducted using the ARTS2 (Eriksson et al., 2011) and QPACK software (Eriksson et al., 2005), following the optimal estimation algorithm (Rodgers, 2000). From the measured spectra, the retrieved water vapor profiles cover an altitude range extending from 37 km to 75 km with a time resolution of 2-4 h and a vertical resolution of 12-19 km. MIAWARA-C measurements were validated against MERRA-2 reanalysis, MLS observations, and WACCM simulations, followed by a comprehensive intercomparison (Schranz et al., 2019, 2020; Shi et al., 2023). Moreover, the effective ascent and descent rates of air were estimated using the water vapor from MIAWARA-C as a passive tracer to investigate the dynamics of transport processes in the Arctic middle atmosphere (Straub et al., 2010; Schranz et al., 2019; Shi et al., 2023).

2.4 Aura-MLS

NASA's Earth Observing System (EOS) Microwave Limb Sounder (MLS) instruments on board the Aura spacecraft measure thermal emissions from the limb of Earth's atmosphere. MLS provides comprehensive measurements of vertical profiles of temperature and 15 chemical species from the upper troposphere to the mesosphere, spanning nearly pole-to-pole coverage from 82°S to 82°N (Waters et al., 2006; Schwartz et al., 2008).

Aura MLS version 5 Level 2 profile measurements of ozone and water vapor VMR between August 2004 and December 2022 are used in this study. The pressure range for MLS ozone measurements useful for scientific applications extends from 215 hPa to 0.001 hPa, while for water vapor it ranges from 316 hPa to 0.001 hPa. The MLS water vapor dataset has been compared globally with ground-based microwave radiometers, typically showing values that are 0–10% higher than the profiles obtained from the microwave radiometers in the range of 3–0.03 hPa (Nedoluha et al., 2017). The ozone profile between MLS and ground-based microwave radiometer measurements agree within 5% in the range of 18–0.04 hPa (Boyd et al., 2007; Bell et al., 2024). Relative differences of ozone and water vapor climatologies at polar stations from Aura-MLS and radiometers agree well, with relative differences mainly within ±7% throughout the middle and upper stratosphere (Shi et al., 2023). In this study, ozone and water vapor profiles are extracted for locations within ±1.2° latitude and ±6° longitude of Ny-Ålesund, Svalbard, Sodankylä, and Tromsø.

2.5 WACCM-X

A comprehensive numerical model, the Whole Atmosphere Community Climate Model with thermosphere and ionosphere extension (WACCM-X), is an atmospheric configuration of the NCAR's Community Earth System Model (CESM) that extends into the thermosphere with a model top boundary between 500 and 700 km (Liu et al., 2018). WACCM-X is capable of being run where the atmosphere is coupled to the active or prescribed ocean, sea ice, and land components, enabling studies at all

https://doi.org/10.5194/egusphere-2024-3749
Preprint. Discussion started: 9 December 2024

atmospheric levels including thermospheric and ionospheric weather and climate. Physical processes represented in WACCM-X are built upon those in regular WACCM configuration, which has a model top at 145 km, which in turn is built upon the Community Atmosphere Model (CAM) with its top at the lower stratosphere. The physics of these models is described in Marsh et al. (2013); Gettelman et al. (2019) and Neale et al. (2013). Both WACCM and WACCM-X include an interactive chemistry module that describes the major chemical processes, including ozone and related chemical tracers. Recent revisions and improvements to WACCM and WACCM-X include new parameterizations of nonorographic gravity wave forcing (Garcia et al., 2017), significant improvements in the frequency of stratospheric sudden warmings (Marsh et al., 2013), chemical kinetic and photochemical rate constants (Sander et al., 2010), and the specification of time-dependent greenhouse gases and ozone-depleting substances (Eyring et al., 2013).

We performed a climatological run leveraging the well-established Specified Dynamics mode of the model (SD-WACCM-X) setup corresponding to the GROMOS-C and MIAWARA-C campaigns. SD-WACCM-X is a version of WACCM-X whose temperature and winds from the surface to the stratosphere at ∼50 km are constrained by the Modern-Era Retrospective Analysis for Research and Applications version 2 (MERRA-2) reanalysis dataset (Gelaro et al., 2017). By nudging with MERRA-2, the model states correspond closely to the actual meteorological state up to the highest nudged altitudes close to the stratopause. The model outputs (winds, temperature, trace gases, and QRL and QRS heating rates) have a conventional latitude-longitude grid with a horizontal resolution of $1.9^\circ \times 2.5^\circ$ and a time resolution of 3 hours. The vertical resolution is the same as WACCM below 0.96 hPa but has been increased to one-quarter scale height above that pressure level. The model top pressure is 4.1×10^{-10} hPa (typically between 500 and 700 km altitude, depending on the solar and geomagnetic activity).

3 Results

3.1 Composite analysis of mean wind response during SSWs

To understand the variation of winds and tides before and after SSW (see Appendix A), the anomalies of zonal and meridional winds and tidal amplitude are investigated. The anomaly is calculated using a climatology based on the same days of all years averaged between 2004 and 2022. Figure 1 presents the composite zonal and meridional wind anomalies observed by three meteor radars at Sodankylä (67.37°N, 26.63°E), Tromsø (69.58°N, 19.22°E), and Svalbard (78.99°N, 15.99°E) as a function of time relative to the SSW central date. The central date was defined according to Li et al. (2023) and can be seen in the SSW Compendium dataset (NOAA CSL, 2024). In the left panel of Figure 1, a reversal of the zonal wind is evident starting about 10 days before the nominal SSW onset according to the mean zonal wind at 10 hPa and 60°N. During this period, the zonal wind becomes westward, with wind reversal anomalies reaching approximately 8 m/s at 80 km altitude.

As we move southward from Svalbard (78.99°N) to Tromsø (69.58°N) and Sodankylä (67.37°N), the altitude of the zonal wind reversal gradually rises, peaking at around 90 km with anomalies reaching up to 20 m/s. Following the onset of the SSW, eastward winds dominate from 80 to 85 km for approximately 45 days, coincidental with the presence of an elevated stratopause that forms after the stratospheric warming and the reformation of the 'normal' stratopause towards the spring transition (Manney et al., 2009; Matthias et al., 2021).

https://doi.org/10.5194/egusphere-2024-3749
Preprint. Discussion started: 9 December 2024

In contrast, the meridional winds at these polar-latitude stations exhibit greater variability than the zonal winds. Alternating positive and negative wind speed anomalies are observed throughout the entire altitude range both before and after the SSW onset (from day -50 to day 20), indicating significant large-scale planetary wave activity in the meridional winds before and during the SSW onset and a reduced activity afterward. Dowdy et al. (2007) and Koushik et al. (2020) have examined the growth and propagation of planetary waves, as well as their interaction with the mean flow, which leads to the reversal of zonal winds and changes in the global mean meridional circulation during SSWs. Planetary wave activity during SSWs plays a crucial role in modulating atmospheric tides (Hibbins et al., 2019; Zhang et al., 2021; van Caspel et al., 2023; Qiao et al., 2024).

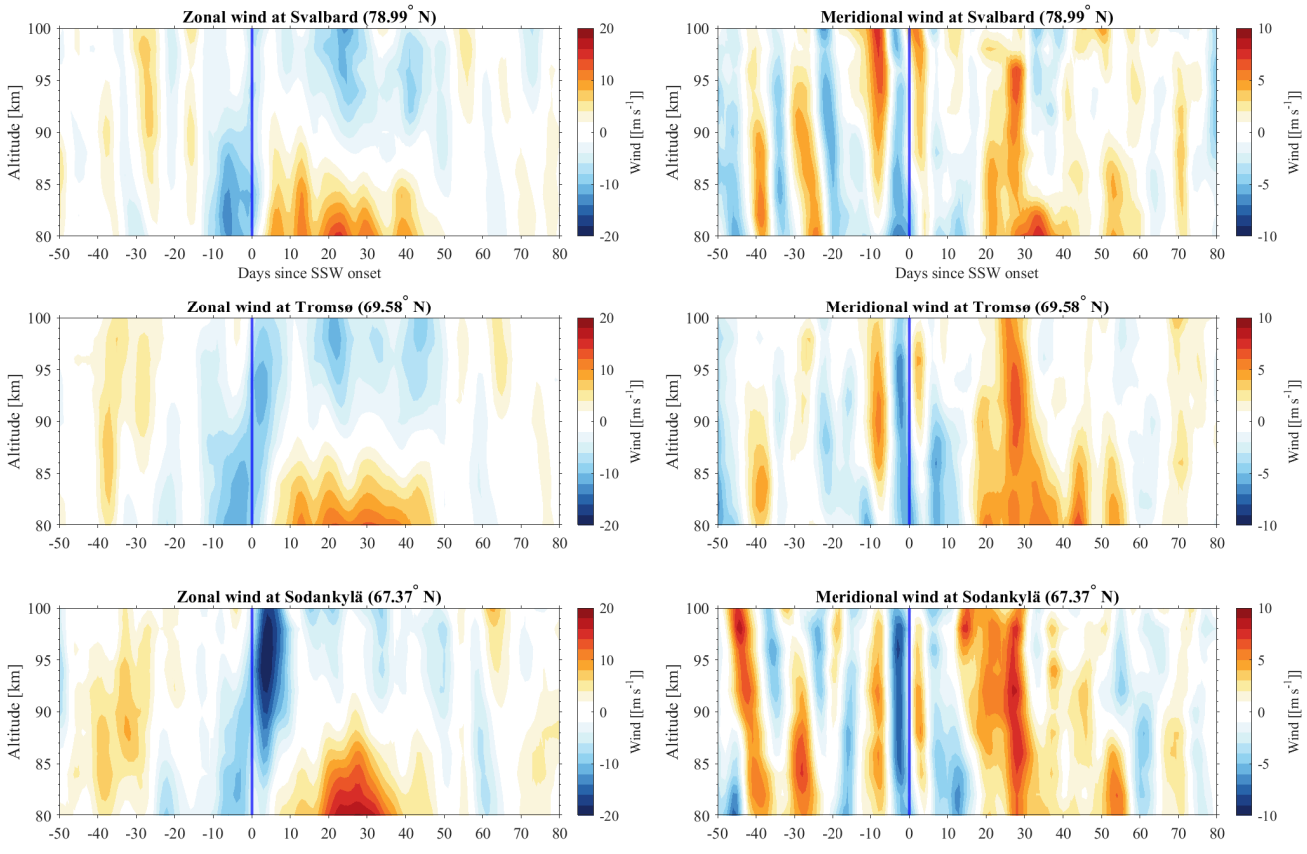

Figure 1. The cross-section of SSW composite zonal (Left panels) and meridional (Right panels) wind anomalies observed with three meteor radars at Sodankylä (67.37°N, 26.63°E), Tromsø (69.58°N, 19.22°E), and Svalbard (78.99°N, 15.99°E) over the period from 2004 to 2021, respectively. The vertical blue line represents the central date of the SSW (day 0 of SSW onset).

https://doi.org/10.5194/egusphere-2024-3749
Preprint. Discussion started: 9 December 2024

3.2 Composite analysis of the mean response of tides during SSW events

The tidal components have been extracted from the zonal and meridional winds observed by meteor radars at the three polar-latitude stations: Tromsø (69.58°N, 19.22°E), Sodankylä (67.37°N, 26.63°E), and Svalbard (78.99°N, 15.99°E) during SSW events, using the procedure discussed in Section 2.1. Figure 2 shows the amplitude anomalies of the TDT in the zonal and meridional winds at these stations, while Figures 3 and 4 illustrate the corresponding anomalies for SDT and DT, respectively. The anomalies show the relative change in amplitude taken as a mean time for the entire showcased period.

In Figure 2, a pronounced decrease in TDT amplitude is observed within a few days before and after the SSW onset, characterized by a magnitude of -4 m/s in both the zonal and meridional wind components. The tidal amplitude changes can be presented as a percentage difference with the mean value. This reduction in TDT amplitude (15-20%) suggests a significant suppression of the TDT during the onset phase of SSWs, possibly due to changes in the background wind and temperature conditions that inhibit the propagation of this tidal mode. Following this initial suppression, TDT amplitudes start to strengthen approximately 10 days after the SSW onset at Svalbard and 20 days later at Tromsø, eventually reaching maximum positive anomalies of up to 4 m/s. The recovery and subsequent amplification of the TDT may be attributed to the reformation of the stratopause and the altered wind structure in the MLT region, which facilitates the upward propagation of the tides. Notably, the strength of the TDT amplitude at Tromsø and Svalbard is stronger than at Sodankylä, indicating potential latitudinal and longitudinal variations in the tidal response to SSWs. These observations align with previous studies that have utilized mechanistic global circulation models (Lilienthal et al., 2018; Lilienthal and Jacobi, 2019) and satellite measurements (Moudden and Forbes, 2013) to discuss the excitation mechanisms of TDT, such as direct solar heating, nonlinear interactions, and gravity wave–tide interactions.

Figure 3 illustrates that the SDT amplitude anomalies at the three stations, in both wind components, can reach up to 10 m/s (changes with peaks reaching up to 40%) within an altitude range of 90-100 km, persisting for only a few days around the SSW onset. This short-lived but intense enhancement of SDT, particularly in the zonal wind component, indicates a strong and rapid response of the SDT to the dynamical changes induced by the SSW. The pronounced increase in SDT amplitudes suggests that the modification of zonal mean winds during SSW may provide more favorable conditions for the upward propagation of SDT, potentially amplified by interactions with planetary waves. This rapid response is also consistent with the ozone enhancement at equatorial to middle latitudes around the onset of the SSW, as shown by Siddiqui et al. (2019) (in Figure 3b). Overall, the SDT amplitude anomalies are found to be approximately twice as large as those of TDT and DT, highlighting the sensitivity of SDT to SSW-induced disturbances. After the peak enhancement, the SDT displays weaker enhancements between 20–50 days after the SSW onset.

Figure 4 shows the DT amplitudes before, during, and after the central date of SSWs. Unlike the TDT and SDT, the DT amplitudes do not exhibit a distinct variation around the SSW onset. However, in both wind components at Sodankylä, Tromsø, and Svalbard, the DT amplitude starts to enhance around 20 days after the SSW onset, reaching a peak nearly 40 days post-SSW. This enhancement in DT amplitude persists for about a month, indicating a delayed response to the SSW. The stronger positive amplitude anomalies are more evident in the meridional wind component than in the zonal wind component. In comparison, the

https://doi.org/10.5194/egusphere-2024-3749
Preprint. Discussion started: 9 December 2024

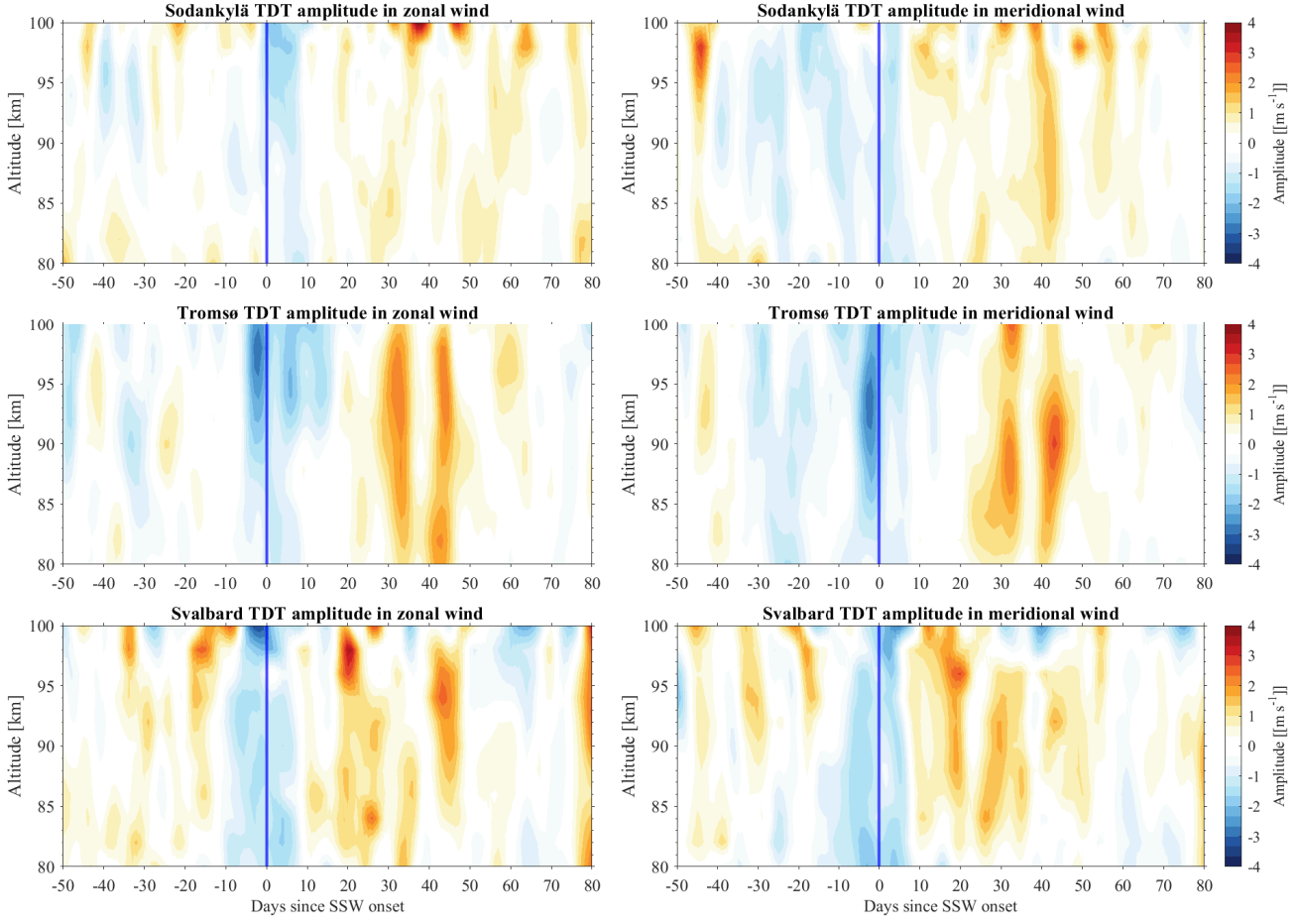

Figure 2. The cross-section of SSW composite TDT amplitude anomalies in the zonal (Left panels) and meridional (Right panels) winds observed with three meteor radars at Sodankylä (67.37°N, 26.63°E), Tromsø (69.58°N, 19.22°E), and Svalbard (78.99°N, 15.99°E), respectively.

positive amplitude anomaly in the zonal wind component above Tromsø and Svalbard is less pronounced than at Sodankylä, suggesting a latitudinal/longitudinal dependency in the DT response. The DT amplitude changes have magnitudes of the order of 30% in the zonal component and 50% in the meridional component. The delayed enhancement of DT could be linked to the gradual restoration of the stratopause and the subsequent changes in thermal and dynamical conditions in the upper mesosphere, which may alter the tidal propagation environment and lead to the amplification of the DT.

3.3 Ozone and water vapor effects on tidal amplitude

Previous studies have identified multiple mechanisms that could contribute to tidal variations during SSW events:

https://doi.org/10.5194/egusphere-2024-3749
Preprint. Discussion started: 9 December 2024

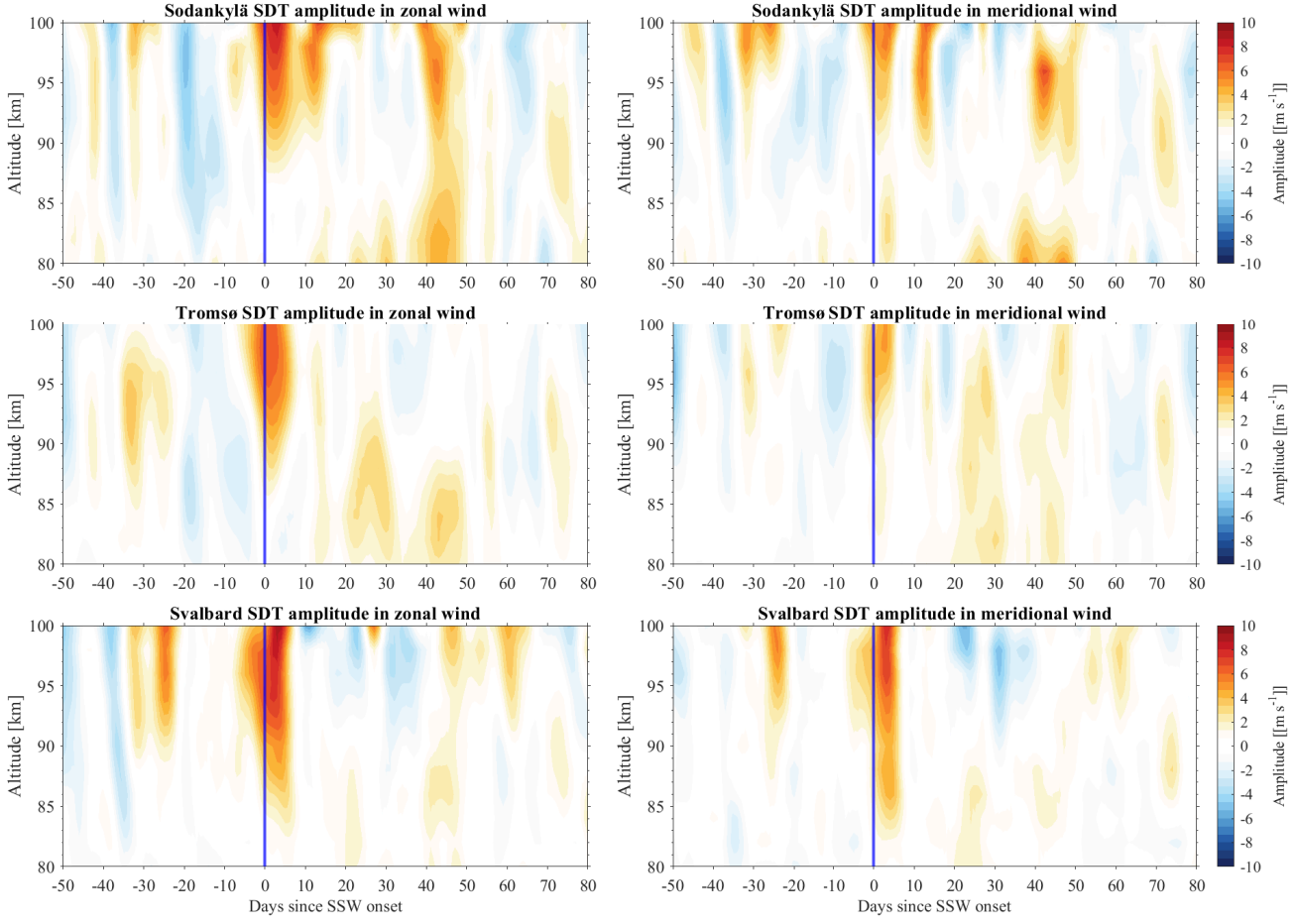

Figure 3. The same as Figure. 2 but for SDT amplitude anomalies.

(a) Changes in the zonal mean winds that influence the vertical propagation of tides in the MLT region (Jin et al., 2012; Pedatella et al., 2012; Stober et al., 2020).

(b) Ozone changes (Goncharenko et al., 2012; Eswaraiah et al., 2018; Siddiqui et al., 2019; Mitra et al., 2024).

(c) Nonlinear interactions between stationary planetary waves and tides (Pedatella and Forbes, 2010; Pedatella and Liu, 2013; Qiao et al., 2024).

In order to explore the effects of ozone and water vapor variability on tidal amplitudes during SSWs, we examine the heating and cooling rates (Figure B1) associated with ozone and water vapor, as well as their connection with the tidal variations. Figure 5 illustrates QRL cooling and QRS heating rate anomalies simulated by the WACCM-X, shedding light on the radiative effects and further helping to quantify the roles of polar ozone and water vapor in modulating mesospheric tide variability during SSWs. The short-wave heating rate in the stratosphere and mesosphere is mainly controlled by ozone through the

https://doi.org/10.5194/egusphere-2024-3749
Preprint. Discussion started: 9 December 2024

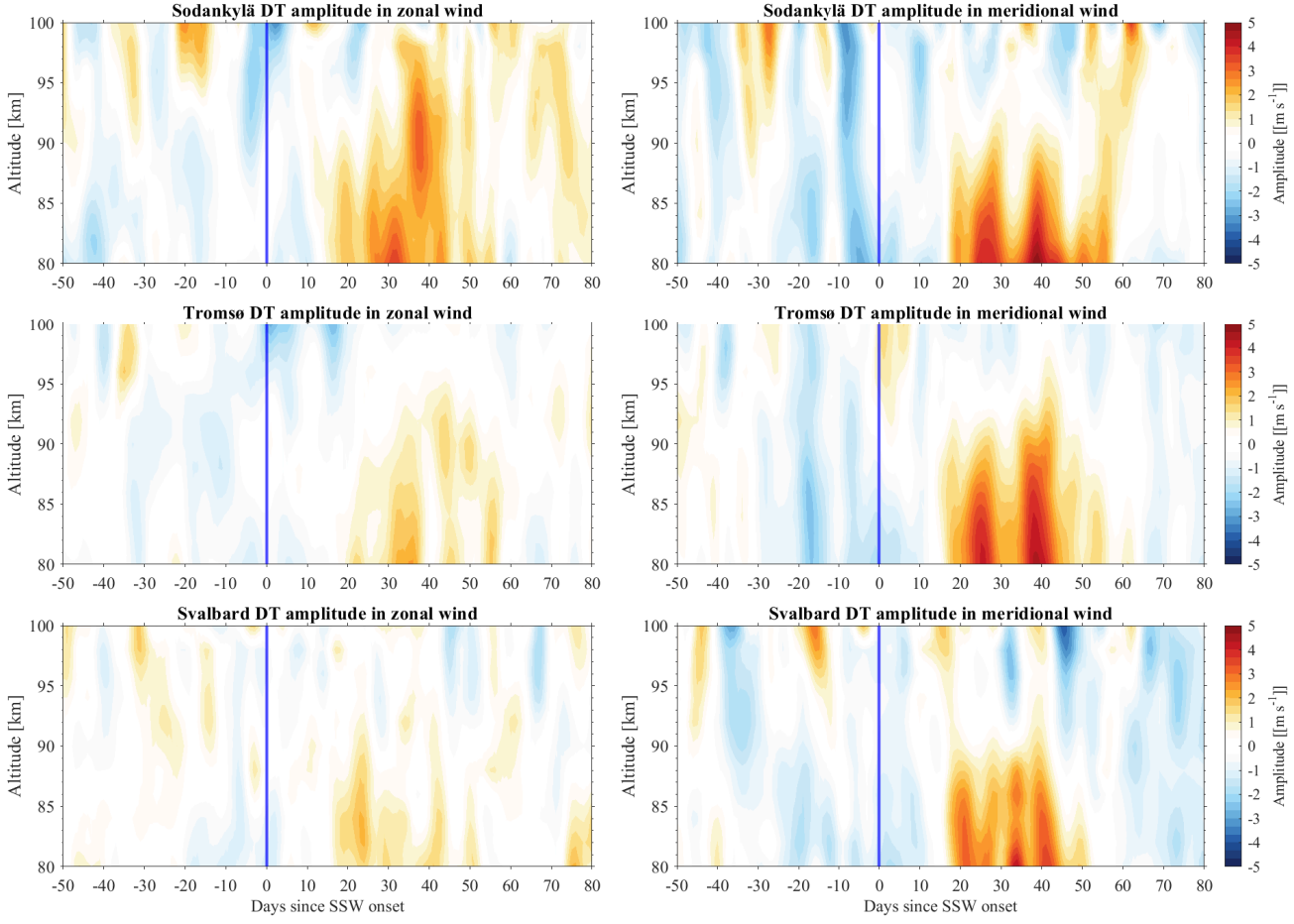

Figure 4. The same as Figure. 2 but for DT amplitude anomalies.

absorption of solar UV radiation. The long-wave cooling rate is associated primarily with the presence of carbon dioxide, with secondary contributions from ozone and water vapor (∼-6 K/day, -2 K/day, and -0.3 K/day, respectively, at 60–70° latitudes in the winter hemisphere and is sensitively dependent on temperature (Brasseur and Solomon, 2005). Figures 6 and 7 present the ozone and water vapor anomalies corresponding to three polar-latitude stations during SSWs, respectively. In Figure 6, the most significant positive ozone anomalies are up to 1.5 ppmv and persist for over 30 days in the middle stratosphere following the SSW onset. In the upper stratosphere and lower mesosphere, positive ozone anomalies persist for approximately two months starting around 10 days after the onset. This indicates a prolonged alteration of the thermal structure of the middle atmosphere during SSW (Schranz et al., 2020). Simultaneously, Figure 7 indicates strong positive water vapor anomalies before and during the SSW onset in the mesosphere, followed by a significant negative anomaly post-SSW. In Figure 8, the ground-based microwave radiometers GROMOS-C and MIAWARA-C effectively capture the variability of ozone and water vapor at Ny-Ålesund, Svalbard during SSW, providing validation for MLS observations and WACCM-X simulations.

https://doi.org/10.5194/egusphere-2024-3749
Preprint. Discussion started: 9 December 2024

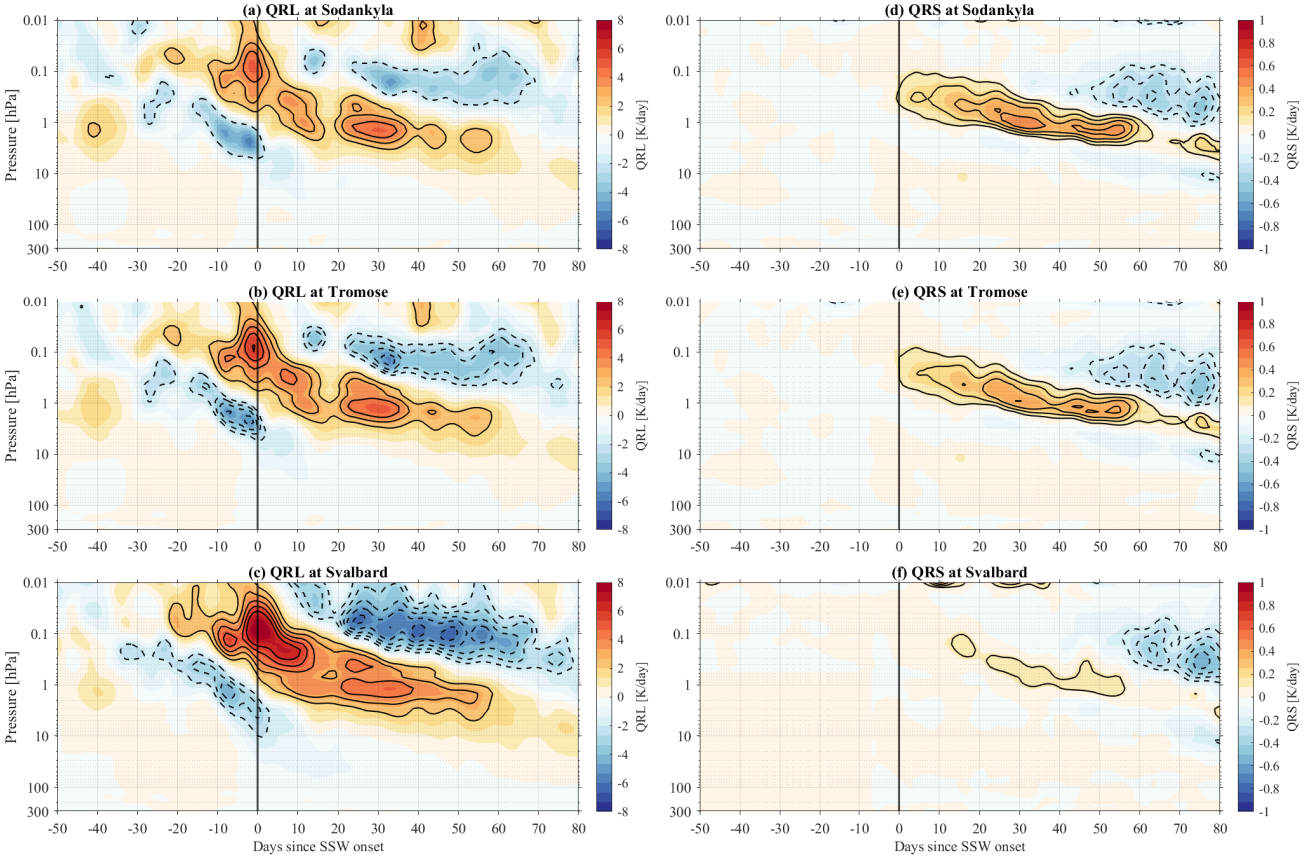

Figure 5. The cross-section of SSW composite QRL cooling and QRS heating rates simulated by WACCM-X over Sodankylä (67.37°N, 26.63°E), Tromsø (69.58°N, 19.22°E), and Svalbard (78.99°N, 15.99°E). The positive and negative anomalies of the QRL (every 1 K/day) and QRS (every 0.1 K/day) rates are shown in solid and dashed contours, respectively. In the left panel, the red area (positive QRL) represents a reduction of cooling, while the blue area (negative QRL) indicates intensified cooling.

The change in ozone is strongly dependent on altitude and latitude, as shown in the measurements and simulations (Figure 6). With the polar wind reversal during the SSW onset, planetary wave activity in the stratosphere drives anomalous equatorial upwelling and cooling that enhances tropical stratospheric ozone. This is qualitatively consistent with findings from Siddiqui et al. (2019) and Limpasuvan et al. (2016), which shows a rapid ozone increase from 20°S to 40°N, and a decrease poleward of 40°N. The ozone enhancement subsequently at mid to high latitudes is consistent with the observational results in Figure 6. The coincidence of the ozone increase at high latitudes, and QRS therein, and the enhancement of SDT may suggest the role of radiative heating by mid-high latitude ozone in the SSW recovery period (day 20-50). The observed ozone increase reaches up to 1.5 ppmv in Figure 6, which is about 50% of the background value. Given that the mean heating rate by ozone at those latitudes is around 1 K/day, the QRS increase shown in Figure 5 is consistent with the ozone change, contributing approximately 0.5 K/day. It is thus reasonable to conclude that the QRS change is mostly due to ozone increase following the

https://doi.org/10.5194/egusphere-2024-3749
Preprint. Discussion started: 9 December 2024

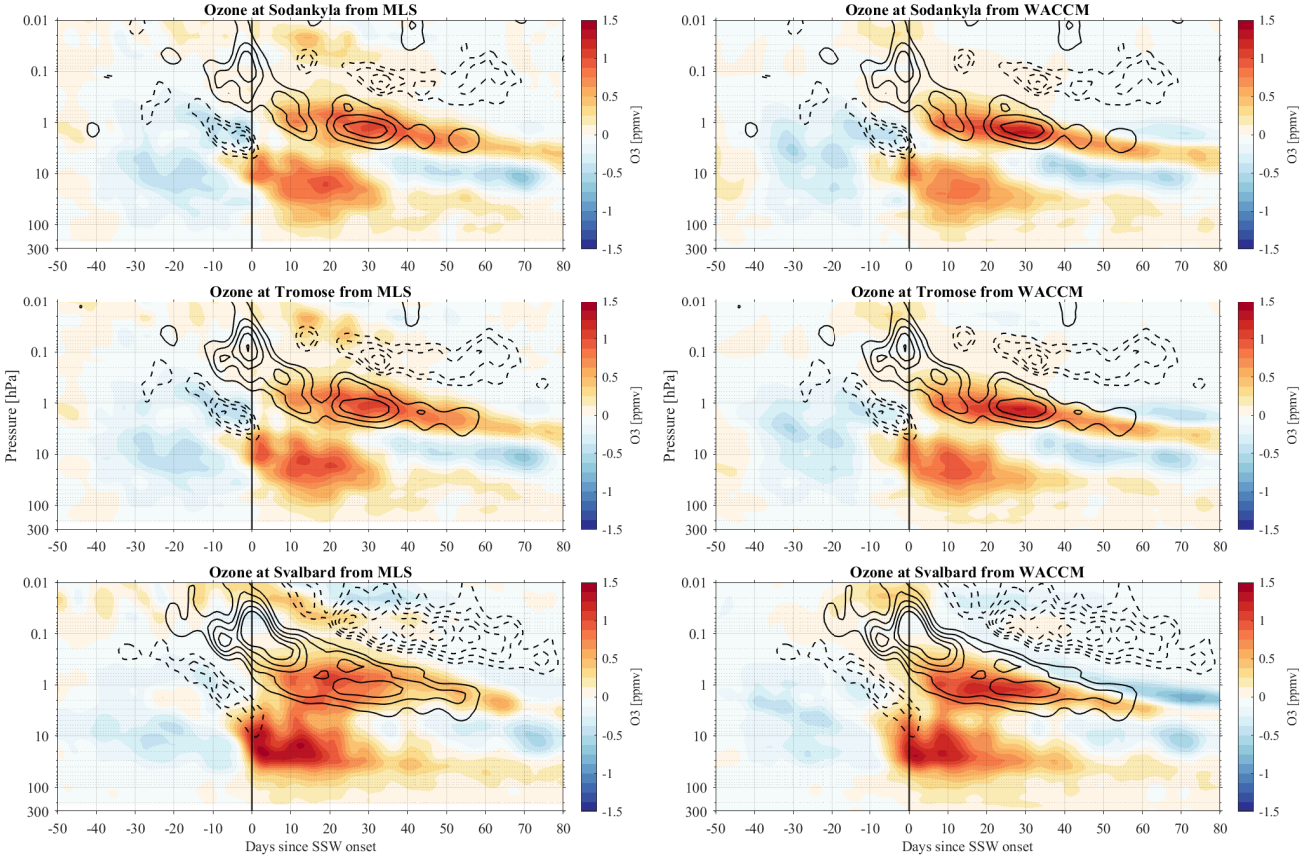

Figure 6. The cross-section of SSW composite ozone anomalies measured by MLS (Left panels) and simulated by WACCM-X (Right panels) over Sodankylä (67.37°N, 26.63°E), Tromsø (69.58°N, 19.22°E), and Svalbard (78.99°N, 15.99°E). The positive and negative anomalies of the QRL (every 1 K/day) rate are shown in solid and dashed contours as in Figure 5, respectively.

SSW. In contrast, SSW-induced changes in water vapor reach up to 25% in Figure 7, translating to changes in cooling rate of about 0.05 K/day. This is negligible compared to the observed absolute QRL cooling rate of up to 5–6 K/day during this period (Figure 5), which is about two orders of magnitude greater. These results demonstrate that water vapor changes are not the primary driver of QRL variations.

Additionally, as shown in Figure 9, the positive (negative) temperature anomalies observed during SSWs reflect dynamical heating (cooling) processes in the stratosphere and mesosphere. To better understand these processes, we calculate dynamical heating and cooling rates associated with the air motion in the Arctic region (65-90°N), along with the long-wave cooling and short-wave heating rates from a diagnostic viewpoint, as shown in Figure 10. The dynamic rates associated with meridional and vertical motions according to the transformed Eulerian mean framework described by equations 3.5.1 in Andrews et al.

https://doi.org/10.5194/egusphere-2024-3749
Preprint. Discussion started: 9 December 2024

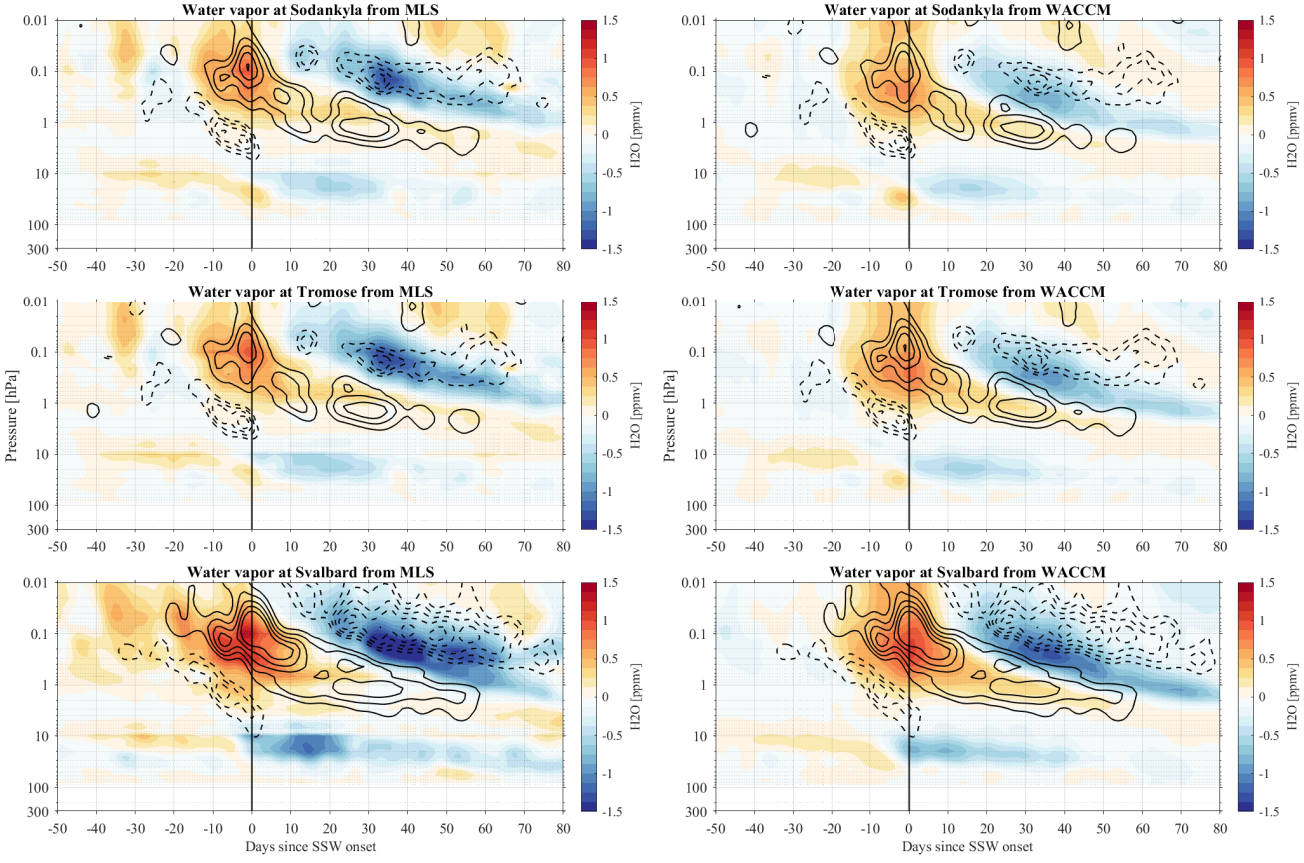

Figure 7. The same as Figure. 6 but for water vapor anomalies.

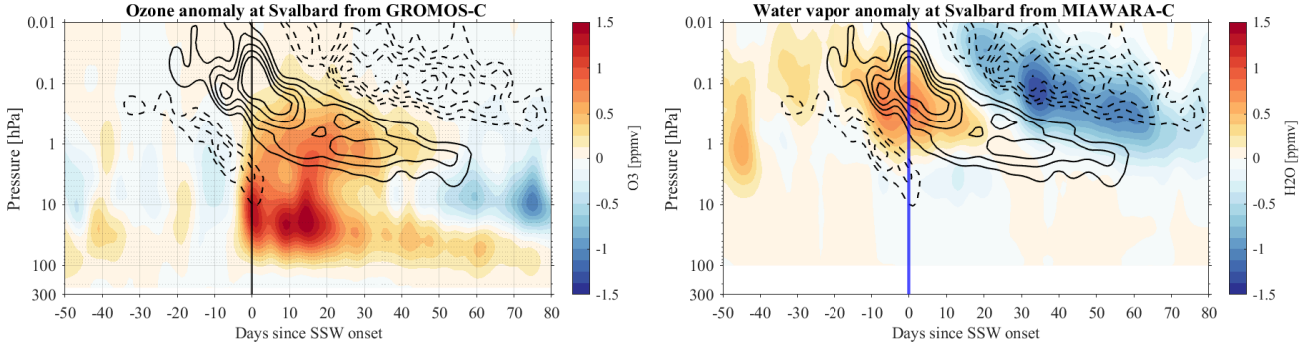

Figure 8. The cross-section of SSW composite ozone and water vapor anomalies from GROMOS-C and MIAWARA-C Ny-Ålesund, Svalbard (78.99°N, 12°E). The positive and negative anomalies of the QRL (every 1 K/day) heating rates are shown in solid and dashed contours, respectively.

https://doi.org/10.5194/egusphere-2024-3749
Preprint. Discussion started: 9 December 2024

(1987) are calculated as follows:

$$Q_{dyn} = -[\overline{v}^* \frac{\partial \overline{T}}{\partial y} + \overline{\omega}^* (\frac{HN^2}{R} + \frac{\partial \overline{T}}{\partial z})] \quad (2)$$

where $\overline{T}$ is the zonally averaged deviation from the global mean temperature, $\frac{\partial \overline{T}}{\partial z}$ represents the temperature gradient, and $\frac{HN^2}{R}$ represents the global mean static stability. Q_{dyn} is the dynamic heating/cooling rate. The $\overline{v}^*$ and $\overline{\omega}^*$ are the residual meridional and vertical winds.

The results indicate that anomalous vertical descent, as shown in Figure B2, causes adiabatic heating in the stratosphere around 10 hPa before the SSW onset, which is only minimally offset by QRL radiative cooling, making the process nearly adiabatic. The upward branch of the enhanced circulation, on the other hand, leads to dynamical cooling in the mesosphere, minimally offset by a reduction in QRL. Although the dynamical heating/cooling term Q_{dyn} dominates in the stratosphere and mesosphere (Figure 10a), the radiative effects from QRL and QRS (Figure 10b, c) play a crucial role in shaping the evolution of the thermal structure of the middle atmosphere. Following the onset of SSW, the dynamic processes drive the persistence of positive ozone anomalies (changes reaching up to 40%) — peaking around day 30 in the upper stratosphere and lower mesosphere—and negative water vapor anomalies (changes reaching up 15%)—peaking around day 35 in the mesosphere. An increase in polar ozone enhances the absorption of UV radiation, as sunlight can enter the stratosphere and lower mesosphere, resulting in heating at these altitudes, while the surface still remains in the Earth's shadow. Thus, the middle atmospheric temperature structure response to SSW is influenced by the ozone. Meanwhile, the dynamic term has a profound and lasting heating effect (with a peak at 0.1 hPa around day 30) on the mesosphere, which is partially countered by enhanced QRL cooling. Therefore, the redistribution of ozone during SSW influences the thermal balance in the middle atmosphere and contributes to the tidal variability during the recovery phase of SSW, as observed in the polar MLT region.

Specifically, the ozone double-layer structure that forms at the onset of the SSW and lasts for about two weeks, results in two layers of substantial UV heating. The superposition of these two diurnal tidal waves at the mesosphere may effectively amplify the SDT at high latitudes due to a 12-hour phase offset caused by the different vertical distances both waves have to travel, considering the typical vertical wavelengths of 30-50 km for semidiurnal tides at this latitude (Stober et al., 2021b). A crucial aspect of marked changes in direct shortwave heating of the stratosphere results from the ozone increase. Therefore, we performed additional analysis by computing the circle of illumination in dependence on altitude. Figure 11 shows a schematic of how to estimate the presence of sunlight for a specific geographic latitude and local time. All calculations are performed using the J2000 reference epoch and the sun ephemerides are valid for the period from 1950 to 2050 (United States Naval Observatory. Nautical Almanac Office and Nautical Almanac Office (U.S.), 2009). The sun is above the horizon at Svalbard at local noon after the 15th of January in the mesosphere and reaches the stratospheric altitudes towards the end of January. At Tromsø and Sodankylä the stratosphere is always illuminated by the sun during noon, although both sites are at latitudes beyond the polar circle and the surface remains in darkness. During midnight all altitudes remain shadowed by the Earth and no sunlight reaches the stratosphere or mesosphere. This characteristic diurnal heating results in pronounced diurnal tide at the stratosphere (Schranz et al., 2018). Thus, the differences in the QRS between Svalbard and the Fennoscandinavian mainland locations are understandable by the availability of direct sunlight for certain altitudes.

https://doi.org/10.5194/egusphere-2024-3749
Preprint. Discussion started: 9 December 2024

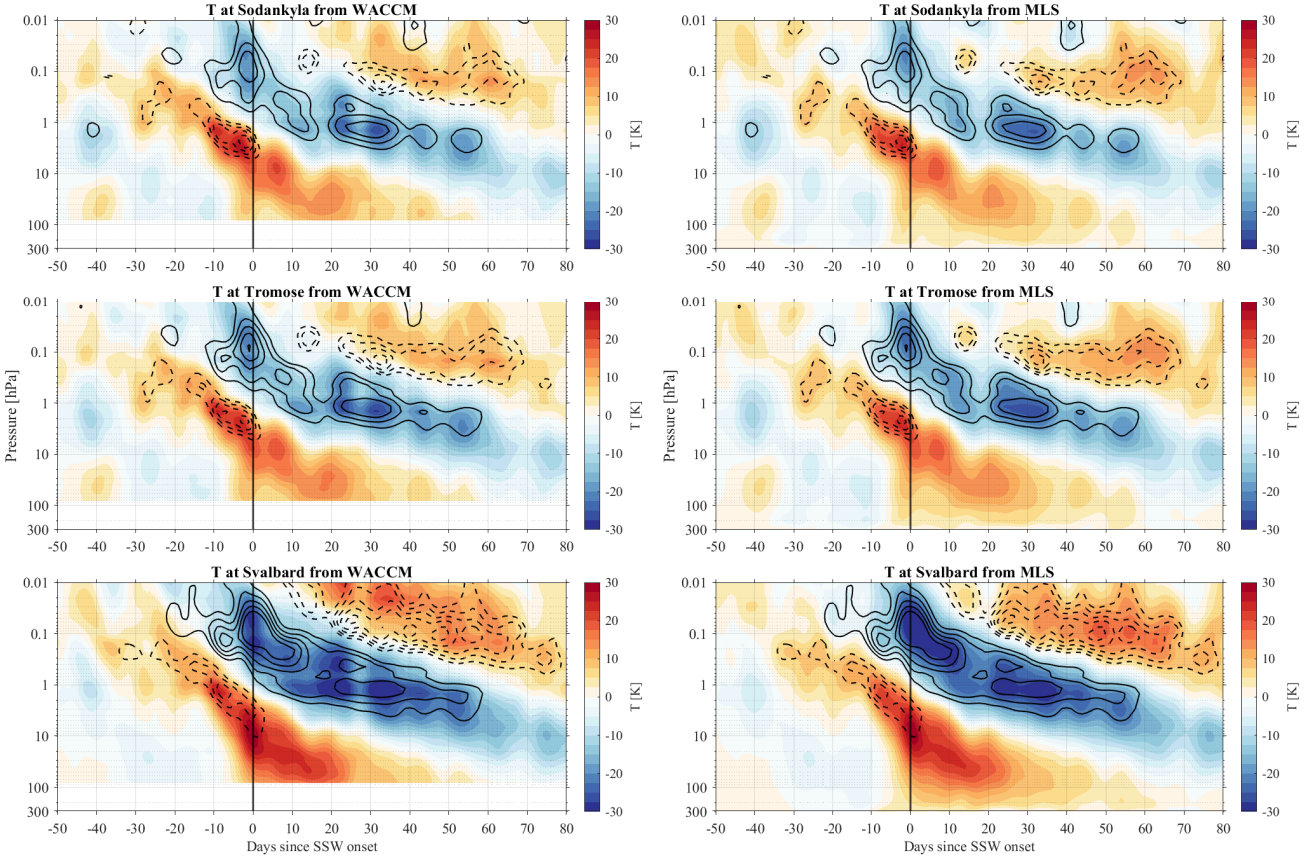

Figure 9. The same as Figure. 6 but for temperature anomalies.

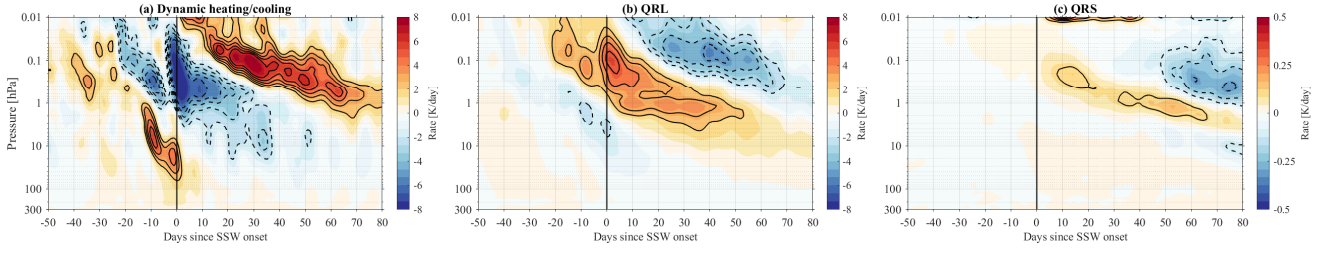

Figure 10. The cross-section of the anomaly of dynamic heating/cooling (Q_{dyn}), QRL, and QRS heating rates averaged over 65-90°N from WACCM-X data.

4 Discussion

This study investigates the amplitude anomalies of DT, SDT, and TDT tides during SSW events using meteor radar data from three polar-latitude stations. The combined analysis of tidal amplitude anomalies and trace gas variations offers new insights

https://doi.org/10.5194/egusphere-2024-3749
Preprint. Discussion started: 9 December 2024

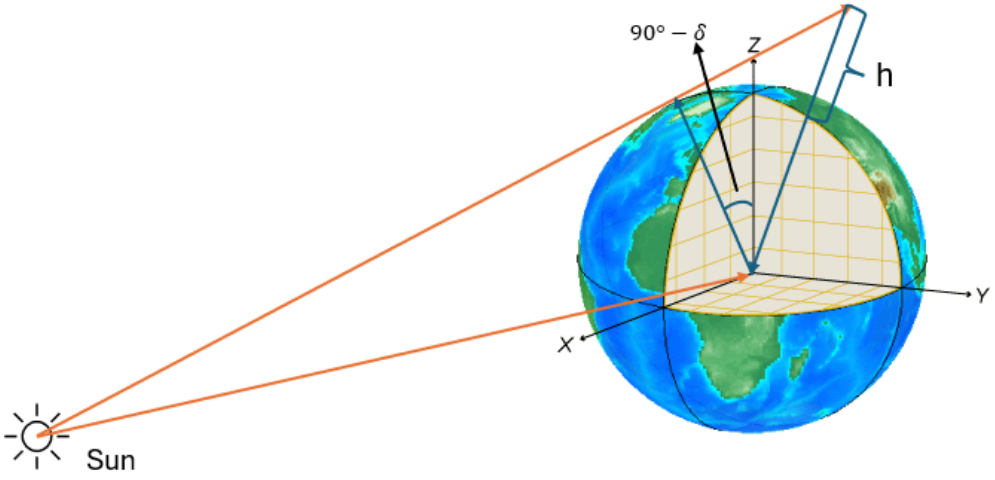

Figure 11. A schematic illustration showing the estimated sunlight presence for a given geographic latitude and local time. The diagram visualizes the variation in sunlight exposure as a function of both latitude and time of day, highlighting the effects of Earth's rotation and axial tilt on day and night cycles.

into the factors influencing tidal dynamics during SSWs, specifically focusing on the role of ozone and water vapor. Our analysis of meteor radar data reveals distinct responses of DT, SDT, and TDT during SSW events. Combining observations and model simulation results represents the first comprehensive attempt to explain mesospheric tidal variability in polar regions during SSWs by highlighting the critical roles of trace gases, and short-wave and long-wave radiative heating and cooling effects as well as dynamic heating/cooling rates associated with horizontal and vertical advection transports.

A significant negative anomaly in TDT amplitudes is observed at the onset of SSWs. In contrast to the TDT, the SDT shows a positive anomaly at the onset of SSWs, indicating that semidiurnal tides are enhanced. This study explores the enhancement of SDT amplitudes at the onset of SSWs, which is primarily attributed to changes in the zonal mean wind and ozone heating at mid-to-low latitudes. Additionally, during the recovery phase, ozone changes at mid-to-high latitudes likely contribute to further modifications in SDT. The dynamical process and long-wave radiative effect primarily determine the mean thermal structure in the mesosphere, as discussed in the previous section. Thus, the immediate responses of SDT tides are most likely driven by dynamical effects and the excitation of the tide at the double-layer ozone structure at the stratosphere and mesosphere, rather than radiative effects related to increased long-wave emissions. In particular, the heating caused by UV absorption appears to be small and is in the order of 0.5 K/day. This is well in the range of observed diurnal tidal temperature amplitudes in the stratosphere (Krochin et al., 2024). However, once excited these tidal modes propagate upward and gain large amplitudes, which helps together with the modified background conditions to amplify the semidiurnal tide at the mesosphere. Thus, the enhancement of up to 40% in the SDT is primarily driven by changing propagation conditions through the background atmosphere and further supported by the double-layer structure of the ozone VMR causing increased UV absorption, consistent with the findings of van Caspel et al. (2023) and Wu et al. (2019). The radiative effect due to ozone becomes more relevant in

https://doi.org/10.5194/egusphere-2024-3749
Preprint. Discussion started: 9 December 2024

the two weeks after the central day of SSW, whereas the dynamic effects dominate during the few days around the onset of the SSW.

The DT exhibits a delayed enhancement, with a positive amplitude anomaly observed approximately 20 days after the onset of the SSW. This peak in DT amplitudes occurs between 80 and 90 km altitude and correlates with both adiabatic heating (which is partially balanced by QRL cooling) and significant ozone VMR changes in the upper stratosphere. The build-up of an elevated stratopause leads to the formation of a distinct double-layer ozone structure in the stratosphere and lower mesosphere, with ozone changes reaching up to 50%. Considering the mean heating rate by ozone at polar latitudes is around 1 K/day (Brasseur and Solomon, 2005), the QRS increase shown in Figure 5 is consistent with the ozone change (<0.5 K/day). It is thus reasonable to conclude that the QRS change is mostly due to ozone increase after SSW onset. The DT tidal enhancement also coincides with the diurnal heating due to the sunlight during this time of the season, which also causes diurnal ozone changes with amplitudes up to 60% in the upper stratosphere (Schranz et al., 2018). Such diurnal ozone changes are related to the forcing of a diurnal temperature tide (Krochin et al., 2024), which reaches a magnitude of 0.5-3 K in the stratosphere with the higher values observed at the stratopause.

One crucial aspect of the presented analysis is the implementation of the adaptive spectral filter technique, which is designed to infer the short-term tidal variability using an adaptive window length for each tidal mode, performing an onion peeling scheme solving first for the mean wind and diurnal tide and other long-period oscillations, which are later used as background regularization for the higher frequency tidal components (Baumgarten and Stober, 2019; Stober et al., 2020). A crucial aspect of the algorithm is that the number of wave cycles determines the window length for each tidal component that is extracted, which in the case of the TDT, SDT and DT is very short resulting in a rather wide band around each tidal frequency and, thus, there could be some contamination due to gravity wave activity that falls into this band. The reduction of TDT amplitude during the SSW might be a combined result of a weakening of the tidal generation plus a change in the GW activity at the stratosphere. A recent study showed that the polar vortex itself can become a source of GWs (Vadas et al., 2024) and, thus, this source is diminishing during the SSW as the polar vortex breaks down.

Our results also confirm the results obtained in van Caspel et al. (2023) using the PRimitive equations In Sigma-coordinates Model (PRISM) tidal model and the Navy Global Environmental Model-High Altitude (NAVGEM-HA) background dynamics to investigate the role of lunar tides relative to the SDT during SSWs. At Svalbard, the lunar tidal amplification should be minimal compared to the mid-latitudes. However, the presented analysis shows a clear SDT amplification after the onset of the SSW similar to Tromsø and Sodankylä, while the lunar tidal potential changes with latitude (Vial and Forbes, 1994; van Caspel et al., 2023). This underlines that radiative effects (heating/cooling) due to the increase/decrease of trace gases such as ozone play a key role in such short-term amplifications and can further amplify dynamical effects altering the vertical tidal propagation during SSWs.

https://doi.org/10.5194/egusphere-2024-3749
Preprint. Discussion started: 9 December 2024

5 Conclusions

This study provides a deeper understanding of the mechanisms driving tidal variability in the polar MLT region during SSW events. The key conclusions from this study are: the meteor radar observations show that the TDT experiences a reduction in amplitude at the onset of SSWs, while the SDT is enhanced. The DT exhibits a delayed enhancement in amplitudes, occurring approximately 20 days after SSW onset coinciding with the presence of an elevated stratopause. These distinct tidal responses highlight the complex interplay between tidal dynamics and atmospheric changes during SSWs. Dynamic heating/cooling rate is partially counteracted by the QRL cooling rate changes, which responds to the temperature change caused by dynamics. The altered background flow creates conditions that are favorable for tidal propagation and amplification, thereby driving the enhancement of SDT amplitude during the SSW.

The SDT tidal enhancement seems to be driven by a complex interplay between the rapid dynamical changes during the onset of SSW and radiative effects supporting the tidal amplification the week after the central day. However, considering that the relative changes in ozone and the change in the SDT tidal amplitude seem to be in the same range of magnitude of 30-40%, it is likely that the radiative effects together with the dynamical effects result in the amplitude amplification. The DT enhancement starting 20 days after the onset of the SSW is likely driven by QRS heating and the preferential condition of the slowly descending elevated stratopause coinciding with an increased ozone VMR reaching relative changes of 30-50% as well, which matches the diurnal tidal pattern in the ozone VMR.

The interaction between trace gas variations, dynamics, radiative effects, and tidal dynamics plays an important role in shaping the response of the MLT region during SSWs. Atmospheric compositions influence the thermal balance through radiative processes, which in turn modulate the propagation and amplitude of tides in polar regions. This study provides a foundation for understanding these interactions, but further research is necessary to explore the coupling between planetary waves, tides, and radiative processes. A better understanding of these dynamics will improve our ability to predict atmospheric responses to major stratospheric events such as SSWs, which have significant implications for space weather and the Earth's upper atmosphere.

Code availability. As a component of the community earth system model, WACCM-X source codes are publicly available at https://www.cesm.ucar.edu/ (NCAR, 2024).

Data availability. MLS v5 data are available from the NASA Goddard Space Flight Center Earth Sciences Data and Information Services Center (GES DISC): https://doi.org/10.5067/Aura/MLS/DATA2516 (Schwartz et al., 2020). The Meteor radar data can be obtained upon request from the instrument PIs. The 3-hourly WACCM-X simulation output is archived on NCAR's archive repository and can be obtained upon request from Guochun Shi. The GROMOS-C and MIAWARA-C level 2 data are provided by the Network for the Detection of Atmospheric Composition Change and are available at https://www-air.larc.nasa.gov/pub/NDACC/PUBLIC/meta/mwave/ (University of

https://doi.org/10.5194/egusphere-2024-3749
Preprint. Discussion started: 9 December 2024

Bern, 2024). NOAA CSL: Chemistry & Climate Processes: SSWC, https://csl.noaa.gov/groups/csl8/sswcompendium/majorevents.html, (last access: October 2024).

Author contributions. GShi was responsible for the WACCM-X simulations, and performed the data analysis, and prepared the manuscript. GStober contributed to the interpretation of the results.NG, MT and AK provided meteor radar data. HL and KW provided their technical assistance in setting up the WACCM-X simulations and DP supported data reduction. All of the authors provided valuable feedback for manuscript editing.

Competing interests. The contact author has declared that none of the authors has any competing interests.

Acknowledgements. Guochun Shi and Gunter Stober are members of the Oeschger Center for Climate Change Research. We acknowledge the PIs for maintaining radar operations. We also thank Joe McInerney for his technical assistance in setting up the WACCM-X simulations, and the National Center for Atmospheric Research for their support during the visit. We thank the Aura/MLS team and NASA/JPL for providing the Microwave Limb Sounding measurements, with the level 2 data set available through the Aura Validation Data Center. This research was supported by the International Space Science Institute (ISSI) in Bern, through ISSI International Team project # 23-580 "Meteors and phenomena at the boundary between Earth's atmosphere and outer space". National Center for Atmospheric Research is a major facility sponsored by the National Science Foundation under Cooperative Agreement No. 1852977.

Financial support. This research has been supported by the Swiss National Science Foundation (grant no. 200021-200517/1) and STFC UK grant (ST/W00089X/1). This research employed data from instruments supported by the Research Council of Norway under the project Svalbard Integrated Arctic Earth Observing System—Infrastructure Development of the Norwegian node (SIOS-InfraNor, Project No. 269927).

Appendix A: Mean winds and tidal amplitudes

Figure A1-A4 show the time variation of the zonal and meridional winds at three sites Sodankylä, Tromsø, and Svalbard, and corresponding TDT, SDT, and DT amplitudes extracted from both wind components. Overlaid contours are better to display the tidal amplitude reductions or enhancements before, during, and after SSW onset.

Appendix B: QRS heating rates and residual vertical wind

In the left panels of Figure B1, the blue regions indicate enhanced cooling, while the red regions represent a reduced cooling rate.

https://doi.org/10.5194/egusphere-2024-3749
Preprint. Discussion started: 9 December 2024

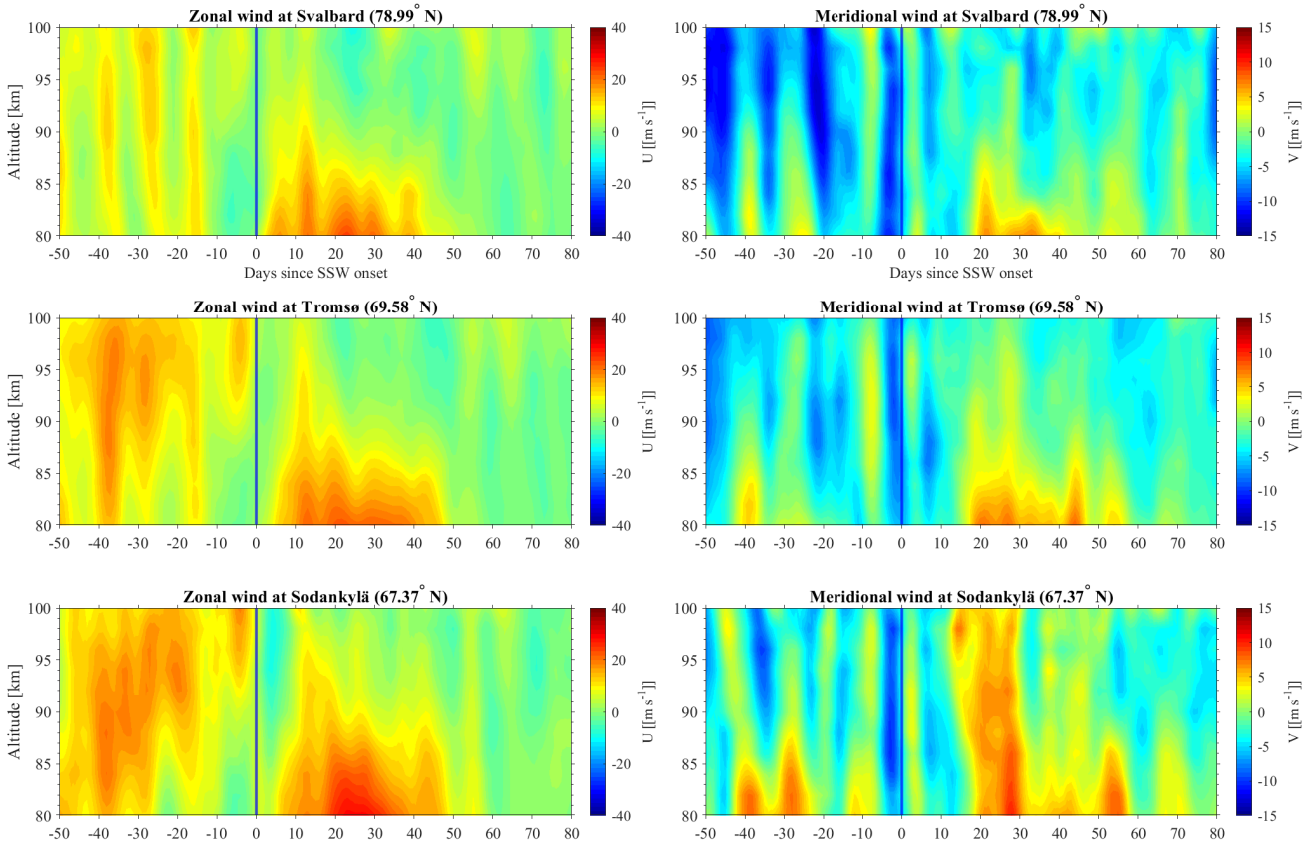

Figure A1. The same as Figure. 1 but for mean zonal and meridional winds.

The residual vertical wind is calculated at each time step using Equation 3.5.1b in Andrews et al. (1987). In the middle stratosphere before day 0, a negative $\overline{\omega}^*$ indicates downwelling, resulting in dynamic heating due to enhanced descent. In the mesosphere at onset, a positive $\overline{\omega}^*$ signifies upwelling, leading to dynamic cooling associated with increased ascent.

https://doi.org/10.5194/egusphere-2024-3749
Preprint. Discussion started: 9 December 2024

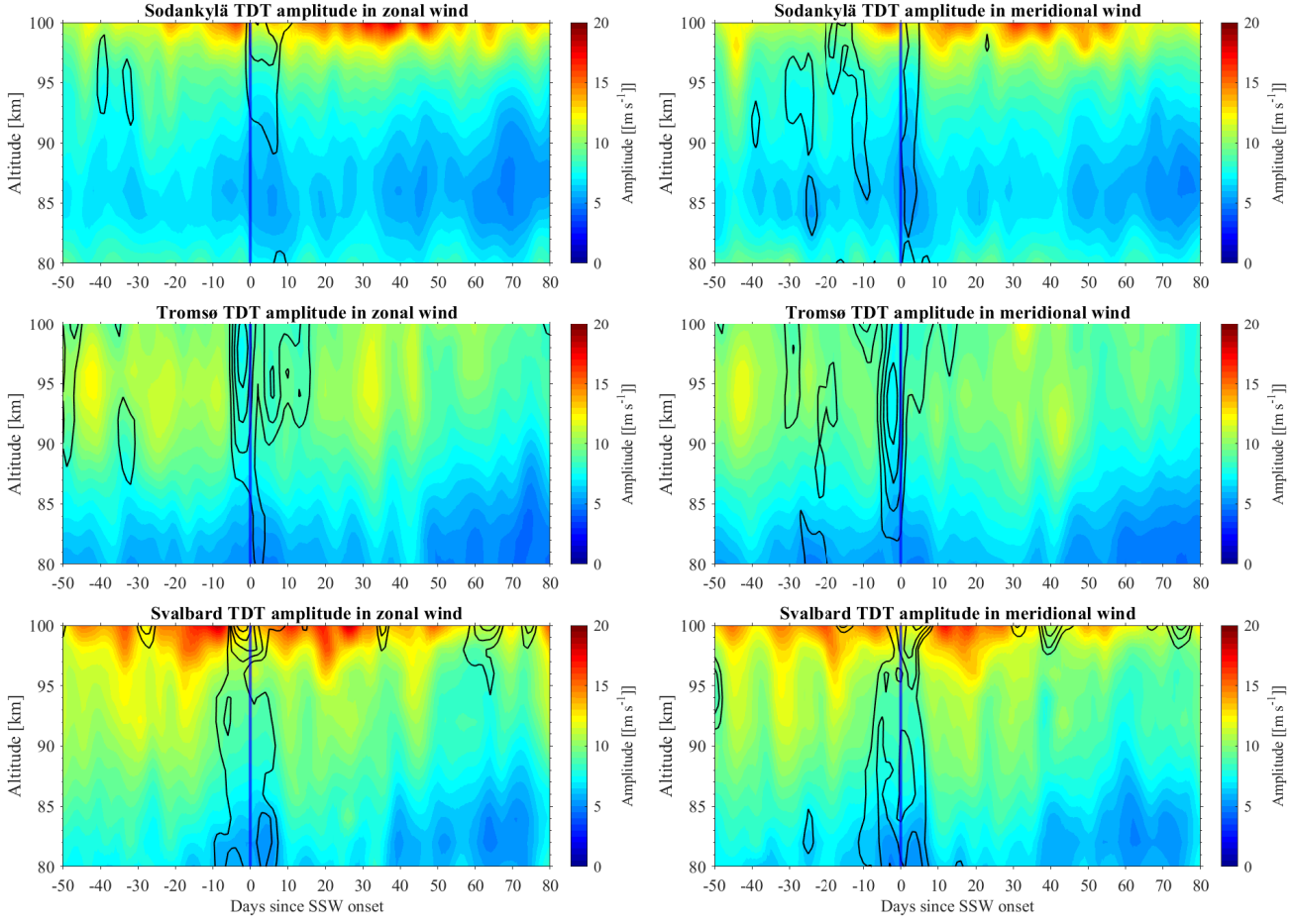

Figure A2. The same as Figure. 2 but for TDT amplitude. Contours represent the TDT amplitude anomlaies.

https://doi.org/10.5194/egusphere-2024-3749
Preprint. Discussion started: 9 December 2024

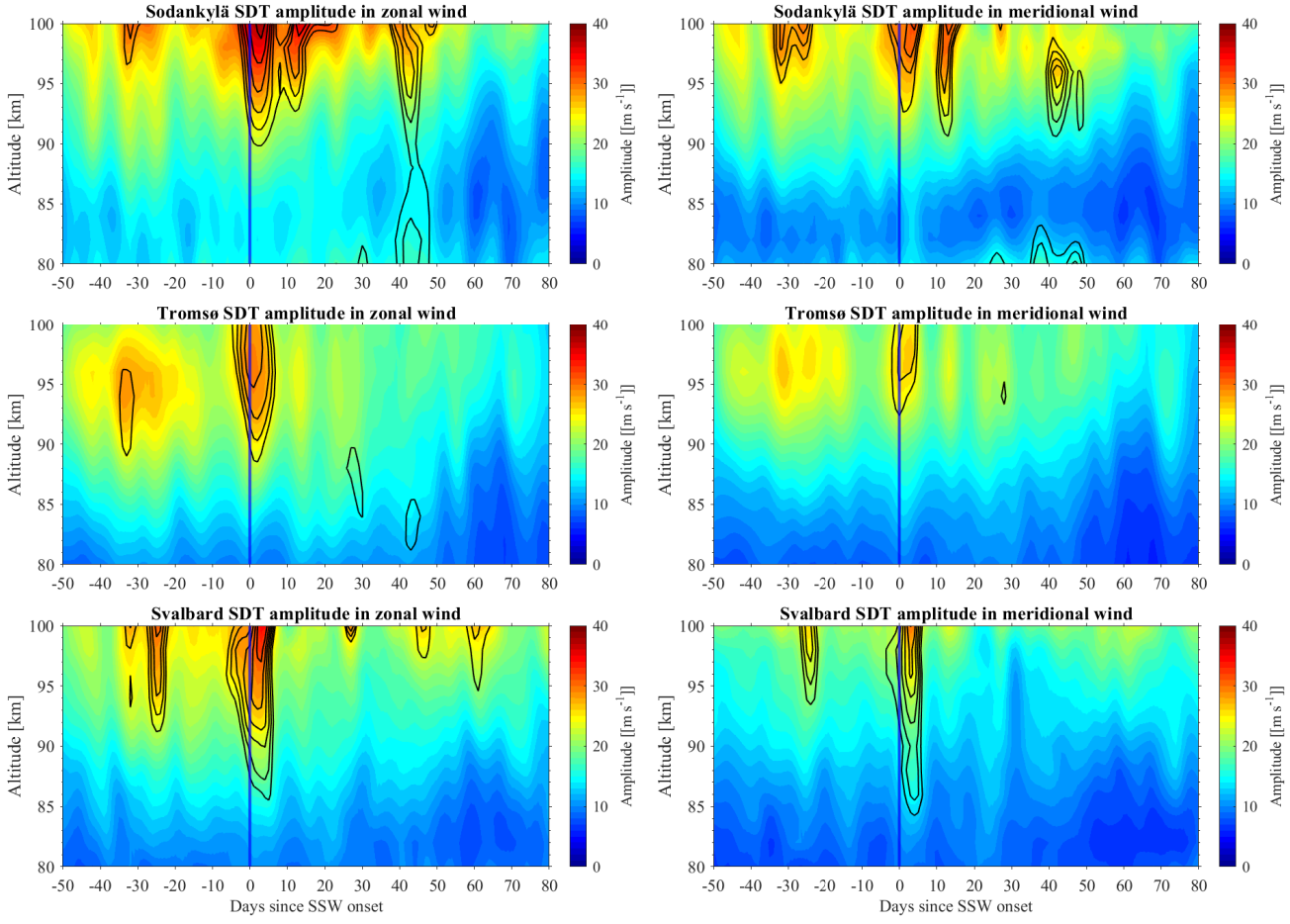

Figure A3. The same as Figure. 3 but for SDT amplitude. Contours represent the SDT amplitude anomlaies.

https://doi.org/10.5194/egusphere-2024-3749
Preprint. Discussion started: 9 December 2024

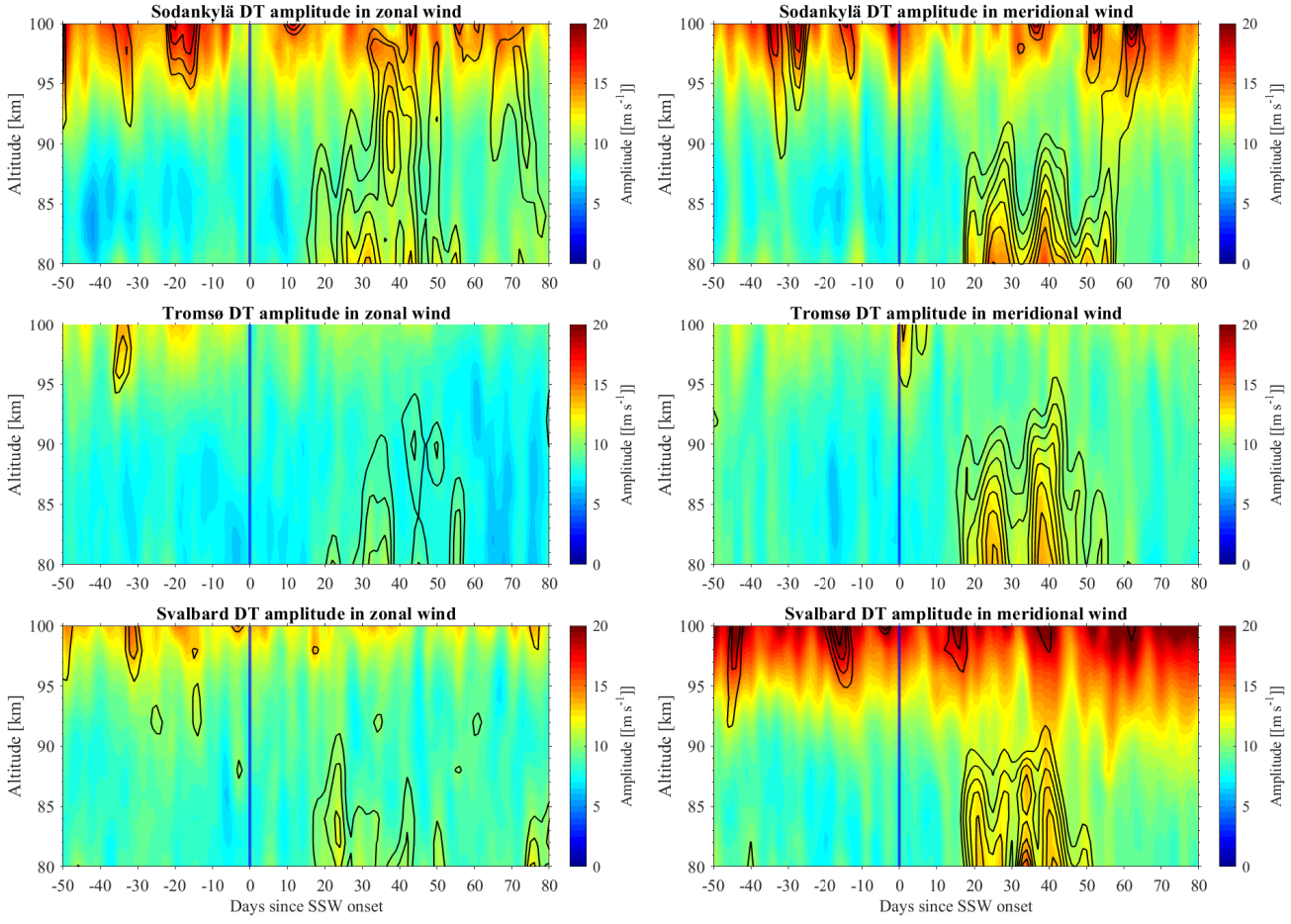

Figure A4. The same as Figure. 3 but for DT amplitude. Contours represent the DT amplitude anomlaies.

https://doi.org/10.5194/egusphere-2024-3749
Preprint. Discussion started: 9 December 2024

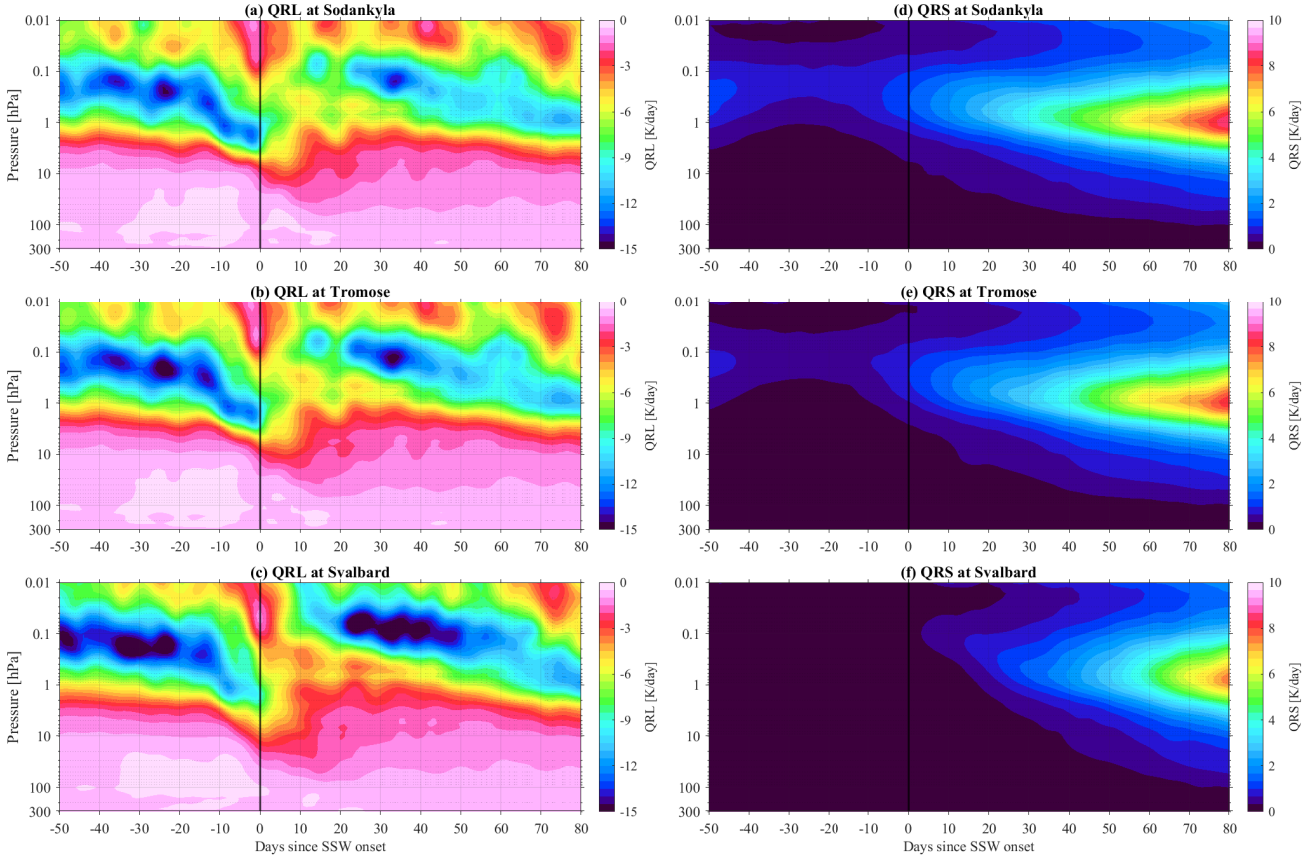

Figure B1. The cross-section of SSW composite of QRL cooling rate (Left panels) and QRS heating rate (Right panels).

https://doi.org/10.5194/egusphere-2024-3749
Preprint. Discussion started: 9 December 2024

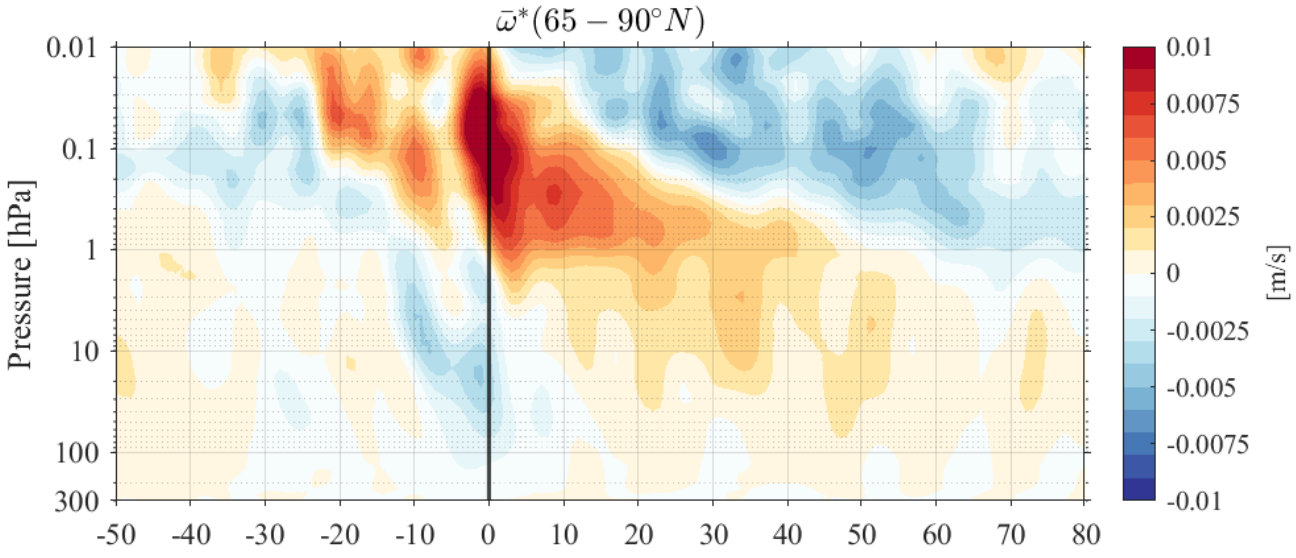

Figure B2. The cross-section of $\bar{\omega}^*$ anomaly during SSW compiste.

https://doi.org/10.5194/egusphere-2024-3749
Preprint. Discussion started: 9 December 2024

References

Andrews, D., Holton, J., and Leovy, C.: Middle Atmosphere Dynamics, International Geophysics, Elsevier Science, 1987.

Bahramvash Shams, S., Walden, V. P., Hannigan, J. W., Randel, W. J., Petropavlovskikh, I. V., Butler, A. H., and de la Cámara, A.: Analyzing ozone variations and uncertainties at high latitudes during sudden stratospheric warming events using MERRA-2, Atmospheric Chemistry and Physics, 22, 5435–5458, https://doi.org/10.5194/acp-22-5435-2022, 2022.

Baldwin, M. P., Ayarzagüena, B., Birner, T., Butchart, N., Butler, A. H., Charlton-Perez, A. J., Domeisen, D. I., Garfinkel, C. I., Garny, H., Gerber, E. P., et al.: Sudden stratospheric warmings, Reviews of Geophysics, 59, e2020RG000 708, 2021.

Baumgarten, K. and Stober, G.: On the evaluation of the phase relation between temperature and wind tides based on ground-based measurements and reanalysis data in the middle atmosphere, Annales Geophysicae, 37, 581–602, https://doi.org/10.5194/angeo-37-581-2019, 2019.

Becker, E.: Mean-Flow Effects of Thermal Tides in the Mesosphere and Lower Thermosphere, Journal of the Atmospheric Sciences, 74, 2043 – 2063, https://doi.org/10.1175/JAS-D-16-0194.1, 2017.

Bell, A., Sauvageat, E., Stober, G., Hocke, K., and Murk, A.: Developments on a 22GHz Microwave Radiometer and Reprocessing of 13-Year Time Series for Water Vapour Studies, EGUsphere, 2024, 1–20, https://doi.org/10.5194/egusphere-2024-2474, 2024.

Bhattacharya, Y., Shepherd, G., and Brown, S.: Variability of atmospheric winds and waves in the Arctic polar mesosphere during a stratospheric sudden warming, Geophysical Research Letters, 31, 2004.

Boyd, I. S., Parrish, A. D., Froidevaux, L., Von Clarmann, T., Kyrölä, E., Russell III, J. M., and Zawodny, J. M.: Ground-based microwave ozone radiometer measurements compared with Aura-MLS v2. 2 and other instruments at two Network for Detection of Atmospheric Composition Change sites, Journal of Geophysical Research: Atmospheres, 112, 2007.

Brasseur, G. P. and Solomon, S.: Aeronomy of the middle atmosphere: Chemistry and physics of the stratosphere and mesosphere, vol. 32, Springer Science & Business Media, 2005.

Chau, J., Hoffmann, P., Pedatella, N., Matthias, V., and Stober, G.: Upper mesospheric lunar tides over middle and high latitudes during sudden stratospheric warming events, Journal of Geophysical Research: Space Physics, 120, 3084–3096, 2015.

Davis, N., Richter, J., Glanville, A., Edwards, J., and LaJoie, E.: Limited surface impacts of the January 2021 sudden stratospheric warming, Nature communications, 13, 1136, 2022.

de la Cámara, A., Abalos, M., Hitchcock, P., Calvo, N., and Garcia, R. R.: Response of Arctic ozone to sudden stratospheric warmings, Atmospheric Chemistry and Physics, 18, 16 499–16 513, https://doi.org/10.5194/acp-18-16499-2018, 2018.

Dempsey, S. M., Hindley, N. P., Moffat-Griffin, T., Wright, C. J., Smith, A. K., Du, J., and Mitchell, N. J.: Winds and tides of the Antarctic mesosphere and lower thermosphere: One year of meteor-radar observations over Rothera (68 S, 68 W) and comparisons with WACCM and eCMAM, Journal of Atmospheric and Solar-Terrestrial Physics, 212, 105 510, 2021.

Domeisen, D. I., Grams, C. M., and Papritz, L.: The role of North Atlantic–European weather regimes in the surface impact of sudden stratospheric warming events, Weather and Climate Dynamics, 1, 373–388, 2020.

Dowdy, A. J., Vincent, R. A., Tsutsumi, M., Igarashi, K., Murayama, Y., Singer, W., Murphy, D. J., and Riggin, D.: Polar mesosphere and lower thermosphere dynamics: 2. Response to sudden stratospheric warmings, Journal of Geophysical Research: Atmospheres, 112, 2007.

Dutta, R., Sridharan, S., and Sinha, P.: Signature of sudden stratospheric warming in the pole and its antipode, Journal of Geophysical Research: Space Physics, 129, e2023JA032 285, 2024.

https://doi.org/10.5194/egusphere-2024-3749
Preprint. Discussion started: 9 December 2024

Eriksson, P., Jiménez, C., and Buehler, S. A.: Qpack, a general tool for instrument simulation and retrieval work, Journal of Quantitative Spectroscopy and Radiative Transfer, 91, 47–64, https://doi.org/https://doi.org/10.1016/j.jqsrt.2004.05.050, 2005.

Eriksson, P., Buehler, S., Davis, C., Emde, C., and Lemke, O.: ARTS, the atmospheric radiative transfer simulator, version 2, Journal of Quantitative Spectroscopy and Radiative Transfer, 112, 1551–1558, https://doi.org/https://doi.org/10.1016/j.jqsrt.2011.03.001, 2011.

Eswaraiah, S., Kim, Y. H., Lee, J., Ratnam, M. V., and Rao, S.: Effect of Southern Hemisphere sudden stratospheric warmings on Antarctica mesospheric tides: First observational study, Journal of Geophysical Research: Space Physics, 123, 2127–2140, 2018.

Eyring, V., Lamarque, J.-F., Hess, P., Arfeuille, F., Bowman, K., Chipperfiel, M. P., Duncan, B., Fiore, A., Gettelman, A., Giorgetta, M. A., et al.: Overview of IGAC/SPARC Chemistry-Climate Model Initiative (CCMI) community simulations in support of upcoming ozone and climate assessments, SPARC newsletter, 40, 48–66, 2013.

Fang, T.-W., Fuller-Rowell, T., Akmaev, R., Wu, F., Wang, H., and Anderson, D.: Longitudinal variation of ionospheric vertical drifts during the 2009 sudden stratospheric warming, Journal of Geophysical Research: Space Physics, 117, 2012.

Fernandez, S., Murk, A., and Kämpfer, N.: GROMOS-C, a novel ground-based microwave radiometer for ozone measurement campaigns, atmospheric measurement techniques, 8, 2649–2662, 2015.

Flury, T., Hocke, K., Haefele, A., Kämpfer, N., and Lehmann, R.: Ozone depletion, water vapor increase, and PSC generation at midlatitudes by the 2008 major stratospheric warming, Journal of Geophysical Research: Atmospheres, 114, 2009.

Forbes, J. M. and Garrett, H. B.: Thermal excitation of atmospheric tides due to insolation absorption by O3 and H2O, Geophysical Research Letters, 5, 1013–1016, 1978.

Garcia, R. R., Smith, A. K., Kinnison, D. E., de la Cámara, Á., and Murphy, D. J.: Modification of the gravity wave parameterization in the Whole Atmosphere Community Climate Model: Motivation and results, Journal of the Atmospheric Sciences, 74, 275–291, 2017.

Gelaro, R., McCarty, W., Suárez, M. J., Todling, R., Molod, A., Takacs, L., Randles, C. A., Darmenov, A., Bosilovich, M. G., Reichle, R., et al.: The modern-era retrospective analysis for research and applications, version 2 (MERRA-2), Journal of climate, 30, 5419–5454, 2017.

Gettelman, A., Mills, M. J., Kinnison, D. E., Garcia, R. R., Smith, A. K., Marsh, D. R., Tilmes, S., Vitt, F., Bardeen, C. G., McInerny, J., Liu, H.-L., Solomon, S. C., Polvani, L. M., Emmons, L. K., Lamarque, J.-F., Richter, J. H., Glanville, A. S., Bacmeister, J. T., Phillips, A. S., Neale, R. B., Simpson, I. R., DuVivier, A. K., Hodzic, A., and Randel, W. J.: The Whole Atmosphere Community Climate Model Version 6 (WACCM6), Journal of Geophysical Research: Atmospheres, 124, 12 380–12 403, https://doi.org/https://doi.org/10.1029/2019JD030943, 2019.

Goncharenko, L., Coster, A., Plumb, R. A., and Domeisen, D. I.: The potential role of stratospheric ozone in the stratosphere-ionosphere coupling during stratospheric warmings, Geophysical Research Letters, 39, 2012.

Günzkofer, F., Pokhotelov, D., Stober, G., Liu, H., Liu, H.-L., Mitchell, N. J., Tjulin, A., and Borries, C.: Determining the Origin of Tidal Oscillations in the Ionospheric Transition Region With EISCAT Radar and Global Simulation Data, Journal of Geophysical Research: Space Physics, 127, e2022JA030 861, https://doi.org/https://doi.org/10.1029/2022JA030861, e2022JA030861 2022JA030861, 2022.

Hall, R. J., Mitchell, D. M., Seviour, W. J., and Wright, C. J.: Tracking the stratosphere-to-surface impact of sudden stratospheric warmings, Journal of Geophysical Research: Atmospheres, 126, e2020JD033 881, 2021.

Haynes, P., McIntyre, M., Shepherd, T., Marks, C., and Shine, K. P.: On the "downward control" of extratropical diabatic circulations by eddy-induced mean zonal forces, Journal of the Atmospheric Sciences, 48, 651–678, 1991.

He, M. and Chau, J. L.: Mesospheric semidiurnal tides and near-12 h waves through jointly analyzing observations of five specular meteor radars from three longitudinal sectors at boreal midlatitudes, Atmospheric Chemistry and Physics, 19, 5993–6006, 2019.

https://doi.org/10.5194/egusphere-2024-3749
Preprint. Discussion started: 9 December 2024

He, M., Chau, J. L., Forbes, J. M., Thorsen, D., Li, G., Siddiqui, T. A., Yamazaki, Y., and Hocking, W. K.: Quasi-10-day wave and semidiurnal tide nonlinear interactions during the Southern Hemispheric SSW 2019 observed in the Northern Hemispheric mesosphere, Geophysical Research Letters, 47, e2020GL091 453, 2020.

Hibbins, R., Espy, P. J., Orsolini, Y., Limpasuvan, V., and Barnes, R.: SuperDARN observations of semidiurnal tidal variability in the MLT and the response to sudden stratospheric warming events, Journal of Geophysical Research: Atmospheres, 124, 4862–4872, 2019.

Hocking, W., Fuller, B., and Vandepeer, B.: Real-time determination of meteor-related parameters utilizing modern digital technology, Journal of Atmospheric and Solar-Terrestrial Physics, 63, 155–169, 2001.

Hoffmann, P., Singer, W., Keuer, D., Hocking, W., Kunze, M., and Murayama, Y.: Latitudinal and longitudinal variability of mesospheric winds and temperatures during stratospheric warming events, Journal of Atmospheric and Solar-Terrestrial Physics, 69, 2355–2366, 2007.

Holdsworth, D. A., Reid, I. M., and Cervera, M. A.: Buckland Park all-sky interferometric meteor radar, Radio Science, 39, n/a–n/a, https://doi.org/10.1029/2003RS003014, rS5009, 2004.

Hong, H.-J. and Reichler, T.: Local and remote response of ozone to Arctic stratospheric circulation extremes, Atmospheric Chemistry and Physics, 21, 1159–1171, https://doi.org/10.5194/acp-21-1159-2021, 2021.

Iida, C., Hirooka, T., and Eguchi, N.: Circulation changes in the stratosphere and mesosphere during the stratospheric sudden warming event in January 2009, Journal of Geophysical Research: Atmospheres, 119, 7104–7115, 2014.

Jacobi, C., Portnyagin, Y. I., Solovjova, T., Hoffmann, P., Singer, W., Fahrutdinova, A., Ishmuratov, R., Beard, A., Mitchell, N., Muller, H., et al.: Climatology of the semidiurnal tide at 52–56 N from ground-based radar wind measurements 1985–1995, Journal of Atmospheric and Solar-Terrestrial Physics, 61, 975–991, 1999.

Jin, H., Miyoshi, Y., Pancheva, D., Mukhtarov, P., Fujiwara, H., and Shinagawa, H.: Response of migrating tides to the stratospheric sudden warming in 2009 and their effects on the ionosphere studied by a whole atmosphere-ionosphere model GAIA with COSMIC and TIMED/SABER observations, Journal of Geophysical Research: Space Physics, 117, 2012.

Koushik, N., Kumar, K. K., Ramkumar, G., Subrahmanyam, K., Kishore Kumar, G., Hocking, W., He, M., and Latteck, R.: Planetary waves in the mesosphere lower thermosphere during stratospheric sudden warming: observations using a network of meteor radars from high to equatorial latitudes, Climate Dynamics, 54, 4059–4074, 2020.

Krochin, W., Murk, A., and Stober, G.: Thermal tides in the middle atmosphere at mid-latitudes measured with a ground-based microwave radiometer, Atmospheric Measurement Techniques, 17, 5015–5028, https://doi.org/10.5194/amt-17-5015-2024, 2024.

Li, Y., Kirchengast, G., Schwaerz, M., and Yuan, Y.: Monitoring sudden stratospheric warmings under climate change since 1980 based on reanalysis data verified by radio occultation, Atmospheric Chemistry and Physics, 23, 1259–1284, 2023.

Lilienthal, F. and Jacobi, C.: Nonlinear forcing mechanisms of the terdiurnal solar tide and their impact on the zonal mean circulation, Annales Geophysicae Discusses, pp. 1–18, 2019.

Lilienthal, F., Jacobi, C., and Geißler, C.: Forcing mechanisms of the terdiurnal tide, Atmospheric Chemistry and Physics, 18, 15 725–15 742, 2018.

Lima, L., Alves, E., Batista, P., Clemesha, B., Medeiros, A., and Buriti, R.: Sudden stratospheric warming effects on the mesospheric tides and 2-day wave dynamics at 7 S, Journal of Atmospheric and Solar-Terrestrial Physics, 78, 99–107, 2012.

Limpasuvan, V., Orsolini, Y. J., Chandran, A., Garcia, R. R., and Smith, A. K.: On the composite response of the MLT to major sudden stratospheric warming events with elevated stratopause, Journal of Geophysical Research: Atmospheres, 121, 4518–4537, 2016.

Lindzen, R. S. and Chapman, S.: Atmospheric tides, Space science reviews, 10, 3–188, 1969.

https://doi.org/10.5194/egusphere-2024-3749
Preprint. Discussion started: 9 December 2024

Liu, G., Lieberman, R. S., Harvey, V. L., Pedatella, N. M., Oberheide, J., Hibbins, R. E., Espy, P. J., and Janches, D.: Tidal variations in the mesosphere and lower thermosphere before, during, and after the 2009 sudden stratospheric warming, Journal of Geophysical Research: Space Physics, 126, e2020JA028 827, 2021.

Liu, G., Janches, D., Ma, J., Lieberman, R. S., Stober, G., Moffat-Griffin, T., Mitchell, N. J., Kim, J.-H., Lee, C., and Murphy, D. J.: Mesosphere and lower thermosphere winds and tidal variations during the 2019 Antarctic sudden stratospheric warming, Journal of Geophysical Research: Space Physics, 127, e2021JA030 177, 2022.

Liu, H.-L., Wang, W., Richmond, A., and Roble, R.: Ionospheric variability due to planetary waves and tides for solar minimum conditions, Journal of Geophysical Research: Space Physics, 115, 2010.

Liu, H.-L., Bardeen, C. G., Foster, B. T., Lauritzen, P., Liu, J., Lu, G., Marsh, D. R., Maute, A., McInerney, J. M., Pedatella, N. M., Qian, L., Richmond, A. D., Roble, R. G., Solomon, S. C., Vitt, F. M., and Wang, W.: Development and Validation of the Whole Atmosphere Community Climate Model With Thermosphere and Ionosphere Extension (WACCM-X 2.0), Journal of Advances in Modeling Earth Systems, 10, 381–402, https://doi.org/10.1002/2017MS001232, 2018.

Manney, G. L., Schwartz, M. J., Krüger, K., Santee, M. L., Pawson, S., Lee, J. N., Daffer, W. H., Fuller, R. A., and Livesey, N. J.: Aura Microwave Limb Sounder observations of dynamics and transport during the record-breaking 2009 Arctic stratospheric major warming, Geophysical Research Letters, 36, 2009.

Marsh, D. R., Mills, M. J., Kinnison, D. E., Lamarque, J.-F., Calvo, N., and Polvani, L. M.: Climate change from 1850 to 2005 simulated in CESM1 (WACCM), Journal of climate, 26, 7372–7391, 2013.

Matsuno, T.: A dynamical model of the sudden stratospheric warming phenomenon, J. Atmos. Sci, 28, 1479–1494, 1971.

Matthias, V., Hoffmann, P., Manson, A., Meek, C., Stober, G., Brown, P., and Rapp, M.: The impact of planetary waves on the latitudinal displacement of sudden stratospheric warmings, Annales Geophysicae, 31, 1397–1415, https://doi.org/10.5194/angeo-31-1397-2013, 2013.

Matthias, V., Stober, G., Kozlovsky, A., Lester, M., Belova, E., and Kero, J.: Vertical Structure of the Arctic Spring Transition in the Middle Atmosphere, Journal of Geophysical Research: Atmospheres, 126, e2020JD034 353, https://doi.org/https://doi.org/10.1029/2020JD034353, e2020JD034353 2020JD034353, 2021.

Mitra, G., Guharay, A., and Paulino, I.: Signature of a zonally symmetric semidiurnal tide during major sudden stratospheric warmings and plausible mechanisms: a case study, Scientific Reports, 14, 23 806, 2024.

Moudden, Y. and Forbes, J.: A decade-long climatology of terdiurnal tides using TIMED/SABER observations, Journal of Geophysical Research: Space Physics, 118, 4534–4550, 2013.

Neale, R. B., Richter, J., Park, S., Lauritzen, P. H., Vavrus, S. J., Rasch, P. J., and Zhang, M.: The mean climate of the Community Atmosphere Model (CAM4) in forced SST and fully coupled experiments, Journal of Climate, 26, 5150–5168, 2013.

Nedoluha, G. E., Kiefer, M., Lossow, S., Gomez, R. M., Kämpfer, N., Lainer, M., Forkman, P., Christensen, O. M., Oh, J. J., Hartogh, P., et al.: The SPARC water vapor assessment II: intercomparison of satellite and ground-based microwave measurements, Atmospheric chemistry and physics, 17, 14 543–14 558, 2017.

Oehrlein, J., Chiodo, G., and Polvani, L. M.: The effect of interactive ozone chemistry on weak and strong stratospheric polar vortex events, Atmospheric Chemistry and Physics, 20, 10 531–10 544, 2020.

Pedatella, N. and Forbes, J.: Evidence for stratosphere sudden warming-ionosphere coupling due to vertically propagating tides, Geophysical Research Letters, 37, 2010.

https://doi.org/10.5194/egusphere-2024-3749
Preprint. Discussion started: 9 December 2024

Pedatella, N. and Liu, H.-L.: The influence of atmospheric tide and planetary wave variability during sudden stratosphere warmings on the low latitude ionosphere, Journal of Geophysical Research: Space Physics, 118, 5333–5347, 2013.

Pedatella, N., Liu, H.-L., Richmond, A., Maute, A., and Fang, T.-W.: Simulations of solar and lunar tidal variability in the mesosphere and lower thermosphere during sudden stratosphere warmings and their influence on the low-latitude ionosphere, Journal of Geophysical Research: Space Physics, 117, 2012.

Pedatella, N., Raeder, K., Anderson, J., and Liu, H.-L.: Ensemble data assimilation in the whole atmosphere community climate model, Journal of Geophysical Research: Atmospheres, 119, 9793–9809, 2014.

Qiao, Z., Liu, A. Z., Pedatella, N., Stober, G., Reid, I. M., Fuentes, J., and Adami, C. L.: Evidence for SSW triggered Q6DW-tide and Q6DW-gravity wave interactions observed by meteor radars at 30 S, Geophysical Research Letters, 51, e2023GL108 066, 2024.

Rodgers, C. D.: Inverse methods for atmospheric sounding: theory and practice, vol. 2, World scientific, 2000.

Sander, S., Friedl, R., Golden, D., Kurylo, M., Moortgat, G., Wine, P., Ravishankara, A., Kolb, C., Molina, M., Finlyason-Pitts, B., et al.: Chemical kinetics and photochemical data for use in atmospheric studies: evaluation number 15, Pasadena, CA: Jet Propulsion Laboratory, California Institute of Technology, 2010.

Sathishkumar, S. and Sridharan, S.: Lunar and solar tidal variabilities in mesospheric winds and EEJ strength over Tirunelveli (8.7 N, 77.8 E) during the 2009 major stratospheric warming, Journal of Geophysical Research: Space Physics, 118, 533–541, 2013.

Schranz, F., Fernandez, S., Kämpfer, N., and Palm, M.: Diurnal variation in middle-atmospheric ozone observed by ground-based microwave radiometry at Ny-Ålesund over 1 year, Atmospheric Chemistry and Physics, 18, 4113–4130, https://doi.org/10.5194/acp-18-4113-2018, 2018.

Schranz, F., Tschanz, B., Rüfenacht, R., Hocke, K., Palm, M., and Kämpfer, N.: Investigation of Arctic middle-atmospheric dynamics using 3 years of H_2O and O_3 measurements from microwave radiometers at Ny-Ålesund, Atmospheric Chemistry and Physics, 19, 9927–9947, https://doi.org/10.5194/acp-19-9927-2019, 2019.

Schranz, F., Hagen, J., Stober, G., Hocke, K., Murk, A., and Kämpfer, N.: Small-scale variability of stratospheric ozone during the sudden stratospheric warming 2018/2019 observed at Ny-Ålesund, Svalbard, Atmospheric chemistry and physics, 20, 10 791–10 806, 2020.

Schwartz, M., Froidevaux, L., Livesey, N., and Read, W.: MLS/Aura Level 2 Ozone (O3) Mixing Ratio V005, Greenbelt, MD, USA, Goddard Earth Sciences Data and Information Services Center (GES DISC), https://doi.org/10.5067/Aura/MLS/DATA2516, 2020.

Schwartz, M. J., Lambert, A., Manney, G. L., Read, W. G., Livesey, N. J., Froidevaux, L., Ao, C. O., Bernath, P. F., Boone, C. D., Cofield, R. E., Daffer, W. H., Drouin, B. J., Fetzer, E. J., Fuller, R. A., Jarnot, R. F., Jiang, J. H., Jiang, Y. B., Knosp, B. W., Krüger, K., Li, J.-L. F., Mlynczak, M. G., Pawson, S., Russell III, J. M., Santee, M. L., Snyder, W. V., Stek, P. C., Thurstans, R. P., Tompkins, A. M., Wagner, P. A., Walker, K. A., Waters, J. W., and Wu, D. L.: Validation of the Aura Microwave Limb Sounder temperature and geopotential height measurements, Journal of Geophysical Research: Atmospheres, 113, https://doi.org/https://doi.org/10.1029/2007JD008783, 2008.

Shi, G., Krochin, W., Sauvageat, E., and Stober, G.: Ozone and water vapor variability in the polar middle atmosphere observed with ground-based microwave radiometers, Atmospheric Chemistry and Physics, 23, 9137–9159, https://doi.org/10.5194/acp-23-9137-2023, 2023.

Shi, G., Krochin, W., Sauvageat, E., and Stober, G.: Ozone anomalies over the polar regions during stratospheric warming events, Atmospheric Chemistry and Physics, 24, 10 187–10 207, 2024.

Siddiqui, T., Maute, A., and Pedatella, N.: On the importance of interactive ozone chemistry in Earth-system models for studying mesosphere-lower thermosphere tidal changes during sudden stratospheric warmings, Journal of Geophysical Research: Space Physics, 124, 10 690–10 707, 2019.

https://doi.org/10.5194/egusphere-2024-3749
Preprint. Discussion started: 9 December 2024

Siddiqui, T. A., Maute, A., Pedatella, N., Yamazaki, Y., Lühr, H., and Stolle, C.: On the variability of the semidiurnal solar and lunar tides of the equatorial electrojet during sudden stratospheric warmings, in: Annales Geophysicae, vol. 36, pp. 1545–1562, Copernicus Publications Göttingen, Germany, 2018.

Sridharan, S., Sathishkumar, S., and Gurubaran, S.: Variabilities of mesospheric tides and equatorial electrojet strength during major stratospheric warming events, in: Annales Geophysicae, vol. 27, pp. 4125–4130, Copernicus Publications Göttingen, Germany, 2009.

Stober, G., Baumgarten, K., McCormack, J. P., Brown, P., and Czarnecki, J.: Comparative study between ground-based observations and NAVGEM-HA analysis data in the mesosphere and lower thermosphere region, Atmospheric Chemistry and Physics, 20, 11 979–12 010, 2020.

Stober, G., Kozlovsky, A., Liu, A., Qiao, Z., Tsutsumi, M., Hall, C., Nozawa, S., Lester, M., Belova, E., Kero, J., Espy, P. J., Hibbins, R. E., and Mitchell, N.: Atmospheric tomography using the Nordic Meteor Radar Cluster and Chilean Observation Network De Meteor Radars: network details and 3D-Var retrieval, Atmospheric Measurement Techniques, 14, 6509–6532, https://doi.org/10.5194/amt-14-6509-2021, 2021a.

Stober, G., Kuchar, A., Pokhotelov, D., Liu, H., Liu, H.-L., Schmidt, H., Jacobi, C., Baumgarten, K., Brown, P., Janches, D., et al.: Interhemispheric differences of mesosphere–lower thermosphere winds and tides investigated from three whole-atmosphere models and meteor radar observations, Atmospheric chemistry and physics, 21, 13 855–13 902, 2021b.

Straub, C., Murk, A., and Kämpfer, N.: MIAWARA-C, a new ground based water vapor radiometer for measurement campaigns, Atmospheric Measurement Techniques, 3, 1271–1285, 2010.

United States Naval Observatory. Nautical Almanac Office and Nautical Almanac Office (U.S.): Astronomical Almanac for the Year 2010 and Its Companion, the Astronomical Almanac Online, Astronomical Almanac for the Year, U.S. Government Printing Office, 2009.

Vadas, S. L., Becker, E., Bossert, K., Hozumi, Y., Stober, G., Harvey, V. L., Baumgarten, G., and Hoffmann, L.: The Role of the Polar Vortex Jet for Secondary and Higher-Order Gravity Waves in the Northern Mesosphere and Thermosphere During 11–14 January 2016, Journal of Geophysical Research: Space Physics, 129, e2024JA032 521, https://doi.org/https://doi.org/10.1029/2024JA032521, e2024JA032521 2024JA032521, 2024.

van Caspel, W. E., Espy, P., Hibbins, R., Stober, G., Brown, P., Jacobi, C., and Kero, J.: A case study of the solar and lunar semidiurnal tide response to the 2013 sudden stratospheric warming, Journal of Geophysical Research: Space Physics, 128, e2023JA031 680, 2023.

Vial, F. and Forbes, J.: Monthly simulations of the lunar semi-diurnal tide, Journal of Atmospheric and Terrestrial Physics, 56, 1591–1607, https://doi.org/https://doi.org/10.1016/0021-9169(94)90089-2, 1994.

Waters, J. W., Froidevaux, L., Harwood, R. S., Jarnot, R. F., Pickett, H. M., Read, W. G., Siegel, P. H., Cofield, R. E., Filipiak, M. J., Flower, D. A., Holden, J. R., Lau, G. K., Livesey, N. J., Manney, G. L., Pumphrey, H. C., Santee, M. L., Wu, D. L., Cuddy, D. T., Lay, R. R., Loo, M. S., Perun, V. S., Schwartz, M. J., Stek, P. C., Thurstans, R. P., Boyles, M. A., Chandra, K. M., Chavez, M. C., Chen, G.-S., Chudasama, B. V., Dodge, R., Fuller, R. A., Girard, M. A., Jiang, J., Jiang, Y., Knosp, B. W., LaBelle, R. C., Lam, J. C., Lee, K., Miller, D., Oswald, J. E., Patel, N. C., Pukala, D. M., Quintero, O., Scaff, D. M., Snyder, W. V., Tope, M. C., Wagner, P. A., and Walch, M. J.: The Earth observing system microwave limb sounder (EOS MLS) on the aura Satellite, IEEE Transactions on Geoscience and Remote Sensing, 44, 1075–1092, 2006.

Wu, Q., Ward, W., Kristoffersen, S., Maute, A., and Liu, J.: Simulation and observation of lunar tide effect on high-latitude, mesospheric and lower thermospheric winds during the 2013 sudden stratospheric warming event, Journal of Geophysical Research: Space Physics, 124, 1283–1291, 2019.

https://doi.org/10.5194/egusphere-2024-3749
Preprint. Discussion started: 9 December 2024

Zhang, J., Limpasuvan, V., Orsolini, Y. J., Espy, P. J., and Hibbins, R. E.: Climatological westward-propagating semidiurnal tides and their composite response to sudden stratospheric warmings in SuperDARN and SD-WACCM-X, Journal of Geophysical Research: Atmospheres, 126, e2020JD032 895, 2021.